Published in final edited form as:

J Immunol. 2021 March 15; 206(6): 1284–1296. doi:10.4049/jimmunol.2000772.

Accelerated clearance and degradation of cell free HIV by neutralizing antibodies occurs via FcγRIIb on liver sinusoidal endothelial cells by endocytosis

James M. Turman[1,†], **Alana M. Cheplowitz**[1,†], **Charu Tiwari**[1,†], **Thushara Thomas**[1,†], **Dhruvi Joshi**[1], **Menakshi Bhat**[2], **Qian Wu**[3], **Erik Pong**[5], **Seung Y. Chu**[5], **David E. Szymkowski**[5], **Amit Sharma**[3], **Stephanie Seveau**[3], **John M. Robinson**[4], **Jesse J. Kwiek**[2], **Dennis Burton**[7], **Murugesan VS. Rajaram**[3], **Jonghan Kim**[6], **Lars Hangartner**[7], **Latha P. Ganesan**[1,*]

[1]Department of Internal Medicine, The Ohio State University, Columbus, OH 43210.

[2]Department of Microbiology and Center for Retrovirus Research, The Ohio State University, Columbus, OH 43210.

[3]Departments of Microbial Infection and Immunity and Veterinary Biosciences, The Ohio State University, Columbus, OH 43210.

[4]Department of Physiology and Cell Biology, The Ohio State University, Columbus, OH 43210.

[5]Xencor, Inc., 111 West Lemon Avenue, Monrovia, CA 91016, USA

[6]Department of Pharmaceutical Sciences, Northeastern University, Boston, MA, USA

[7]Department of Immunology and Microbial Science, The Scripps Research Institute, La Jolla, CA 92037.

Abstract

Neutralizing antibodies suppress HIV infection by accelerating viral clearance from blood circulation, in addition to neutralization. The elimination mechanism is largely unknown. We determined that human liver sinusoidal endothelial cells (LSEC) express FcγRIIb as the lone Fc gamma receptor, and, using humanized FcγRIIb mouse, we found that antibody-opsonized HIV pseudoviruses (Ab-HIV) were cleared considerably faster from circulation than HIV by LSEC FcγRIIb. Compared to humanized FcγRIIb expressing mice, HIV clearance was significantly slower in FcγRIIb KO mice. Interestingly, pentamix of neutralizing antibodies cleared HIV faster compared to polyclonal HIVIG, though the HIV antibody-antigen ratio was higher in immune complexes made of HIVIG and HIV than pentamix and HIV. The effector mechanism of LSEC FcγRIIb was identified to be endocytosis. Once endocytosed, both Ab-HIV and HIV localized to lysosomes. This suggests that clearance of HIV, endocytosis and lysosomal trafficking within LSEC occur sequentially, and that the clearance rate may influence downstream events. Most importantly, we have identified LSEC FcγRIIb-mediated endocytosis to be the Fc effector

[*]**CORRESPONDING AUTHOR:** Dr. Latha P. Ganesan, Department of Internal Medicine, Division of Immunology and Rheumatology & Division of Nephrology, The Ohio State University, 510 DHLRI, 473 West 12th Avenue, Columbus, OH 43210. Phone: (614) 247-7650; Fax: (614) 247-7669; Latha.Ganesan@osumc.edu.
[†]These authors contributed equally to this work

mechanism to eliminate cell free HIV by antibodies, which could inform development of HIV vaccine and antibody therapy.

Keywords

HIV; effector functions; FcγR; endocytosis; lysosomes; phagocytosis; lamp1; HIV Ab therapy; clearance; HIVIG; Kupffer cells; liver; Liver sinusoidal endothelial cell; innate immune function; Fc effector function; elimination; HIV degradation; inhibitory receptor; activation; HIV immunotherapy; HIV vaccine; neutralizing antibodies; non-neutralizing antibodies; immune complex

INTRODUCTION:

Increased HIV drug-resistance and increased mortality associated with HIV infections have prompted new approaches to HIV immunotherapy. The treatment of viral infections, including HIV, involve anti-viral antibodies (Abs) (1). For example, administration of cocktails of HIV-specific neutralizing antibodies (NAbs), as well as the single NAb PGT121 or b12, cause a rapid and precipitous decline of viremia to undetectable levels in macaques (2, 3). Furthermore, improvements in HIV vaccine design benefit from a detailed understanding of *in vivo* actions of anti-HIV Abs. Given the potential for Abs in HIV immunotherapy, a better understanding of the mechanisms of Ab-mediated actions should help to optimize such therapies.

A currently accepted *in vivo* mechanism of action of anti-HIV Abs involves accelerating the clearance of cell-free HIV virions from systemic blood circulation (4). Here, anti-HIV Abs binds HIV to form immune complex, which in turn, binds to immune cell surface Fc receptors for IgG (FcγR) and becomes a target for complement binding. Binding to FcγR, but not to complement, appears to be helpful in some protection against HIV, *in vivo* by bnAbs (3) but was found to be dispensable for others(5). Given the existence of multiple FcγRs, a key unanswered question concerns the roles of the various FcγR involved in clearing the Ab-opsonized cell-free HIV. An additional open question concerns the effector mechanisms of Ab-opsonized HIV uptake and degradation.

FcγRs are integral cell membrane glycoproteins with receptor type-specific distinguishing features. In humans, the FcγR family consists of three major types, namely FcγRI/CD64, FcγRII/CD32, and FcγRIII/CD16(6). FcγRI and FcγRIII perform agonist/activation functions via their association with a γ-subunit (the FcRγ chain) containing an Immunoreceptor Tyrosine-based Activation Motif (ITAM) in its cytoplasmic domain. By contrast, FcγRIIa carries its own ITAM as an integral part of the cytoplasmic domain (7). FcγRIIa, which appears to be unique to primates, is a low-affinity activating receptor. The final known human family member, FcγRIIb, is a single polypeptide chain with a cytoplasmic tail containing an Immuno-Tyrosine based Inhibitory Motif (ITIM). In B-cells, dendritic cells, macrophages,and neutrophils. FcγRIIb ITIM offers negative feedback for the signaling generated by activating FcγR when co-expressed with ITAM in the same cell (8, 9). It is therefore referred to as an (or the) “inhibitory receptor”.

Recently our group discovered that, of the four types of mouse FcγR, one form, FcγRIIb, is expressed abundantly in mouse liver (10). In mice, we observed that 75% of the total body FcγRIIb is expressed in liver, specifically in liver sinusoidal endothelial cells (LSEC). Functionally, FcγRIIb is known to clear small immune complexes (SIC). Given that Ab-opsonized HIV reportedly falls into the category of SIC, as measured by dynamic light scattering (HIV alone 150nm and HIV opsonized with IgG to a maximum 170nm), these complexes are the appropriate size for receptor-mediated endocytosis by LSEC (11, 12).

Liver is known to be the major organ for clearing viruses such as SIV (13) and HIV (14). The major cell type in liver responsible for clearance is LSEC, in the case of HIV-like and Ad5 particles at an astonishingly rapid rate (15, 16). LSEC are well equipped for vigorous endocytosis in that they express major endocytic receptors including scavenger receptors (17–19).

Although much is known about the Fc effector mechanisms such as phagocytosis and ADCC, which clear HIV-infected cells via macrophages and NK cells, the Fc effector function that eliminates Ab-opsonized cell free HIV from systemic circulation remain obscure. One hurdle to this understanding involves the assumption that the relevant Fc effector mechanism is phagocytosis. However, the HIV Envelope (Env) is, in fact, a poor target for phagocytosis, having only 8–10 surface Env trimmers capable of Ab binding to form immune complexes of more than few μm(20, 21). Instead, these smaller complexes are typically engulfed via endocytosis. Phagocytosis involves uptake of particles larger 0.5 μm by a process involving actin polymerization; endocytosis, by contrast, is defined as uptake of small, i.e. <0.5, particles into vesicles via a process that does not involve actin polymerization.

Anti-HIV Abs can be neutralizing (NAbs) or non-neutralizing (non-NAbs). NAbs bind and inactivate viruses though their Fab regions. Thus, NAbs block HIV attachment to target cells by interfering with the interaction between HIV and its cellular receptors, such as the CD4 or CCR5/CXCR4 binding sites on gp120. NAbs also block HIV entry and thus prevent infection *in vitro*(22). However, the *in vivo* protective ability of NAbs are complex and involve clearance mediated by the innate immune system (23). Both NAbs and non-NAbs employ their Fc domains to activate immune cells and thus may interact equally with FcγR-expressing cells (24).

Drawing on the evidence presented above, we propose and confirm our hypothesis that NAbs clear HIV from circulation via endocytosis by FcγRIIb on LSEC. To assess the function of human FcγRIIb for clearing human Ab-HIV, we generated a humanized FcγRIIb knock-in mouse strain (2B-KIX) wherein the extracellular domain of the mouse FcγRIIb gene sequence was replaced with the sequence for the human extracellular domain. To study HIV clearance, we used both pseudotyped single cycle HIV (HIV) and HIV virus-like particles (HIV-LP) as they express the same HIV Env to which the Abs bind.

MATERIALS AND METHODS:

Animals.

Wild-type BALB/c male mice ages 12–16 weeks were obtained from The Jackson Laboratory. Transgenic mice expressing human FcγRIIb, 2B-KIX, from Xencor were breed and maintained. FcγRIIb knock-out mice in C57BL/6 background (Dr. Jeffrey Ravetch) were purchased from The Jackson Laboratory. All studies were approved by The Ohio State University Institutional Animal Care and Use Committee and all procedures were in accordance with their guidelines. All surgery was performed under Isoflurane anesthesia, and all efforts were made to minimize suffering.

Antibodies.

The following anti-FcγR Abs were used: For immunofluorescence KB61 (IgG1; D. Mason, Radcliffe Hospital, Oxford, U.K) was used at a working concentration at 10μg/ml. For flow cytometry, the mouse anti-human FcγRIIb/c Ab, 4F5 (25) was used at 10μg/ml. For immunoblotting, protein G purified IgG of rabbit polyclonal Ab 260 was used to detect FcγRIIa while a rabbit anti-FcγRIIb antibody from Novus Biologicals was used to detect both b1 and b2.

The other primary Abs used for flow cytometry, immunofluorescence and immunoblotting are anti-CD68 Ab (IgG2b, κ; Biolegend), Rabbit anti-FcεRI γ subunit Ab (EMD Millipore), anti-mouse CD206 Ab (Santa Cruz), anti-mouse F4/80 Ab (Abd Serotec), anti-mouse CD16/CD32 Ab (BD Pharmigen), mouse anti-human CD64 (Biolegend), mouse anti-human CD16 (Biolegend) mouse anti-GAPDH mab (6C5) (Santa Cruz), 2.4G2 PE-Cy7 (BD Pharmigen), F4/80 PE (eBioscience), NK-1.1 FITC (Biolegend), Desmin Pac-blue (Thermoscientific), and Cd11c PerCP (Biolegend). The isotype controls used are ChromPure normal rat IgG, normal rabbit IgG, normal goat IgG (Jackson ImmunoResearch), normal mouse IgG (Santa Cruz), mouse IgG1κ (Biolegend) and mouse IgG2b, κ (Jackson ImmunoResearch), IgG2b.κ PE-Cy7 (BD Pharmingen), IgG2a.κ PE (eBioscience), IgG2a.κ FITC (Biolegend), anti-Rab 405 (Jackson ImmunoResearch), and American Hamster IgG Percp (Biolegend).

The secondary Abs used for immunofluorescence were Goat F(ab)'$_2$ anti-mouse IgG 488 and AffiniPure Donkey Anti-Rabbit IgG DyLight 405 Ab from Jackson ImmunoResearch. The goat anti-mouse IgG 594, Goat anti-Rabbit IgG 488, Goat anti-Rabbit IgG 594 and Goat anti-Rat IgG 647 Abs were from Invitrogen.

Tissue procurement and preparation.

Healthy human liver samples, identified only by patient sex and age, were procured from the Cooperative Human Tissue Network, Midwestern Division at The Ohio State University. The Institutional review board (The Ohio State University) determined that this study did not qualify as human subject research.

The liver tissues were cut into 3–4 mm^3 pieces, rinsed in cold PBS, and fixed in 4% paraformaldehyde in PBS (with 0.02% sodium azide) at room temperature for 2 hours. The fixed samples were washed with PBS for a total of 2 hours. Tissues were then incubated

with 20% sucrose in PBS for 8–16 hours. The samples were then placed in TBS freeze medium in molds and stored in −80°C until sectioning.

2B-KIX mouse generation.

The humanization of the mouse FcγRIIb extracellular domain was achieved by replacing the FcγRIIb mouse equivalent genomic sequence leading to the expression of a chimeric protein containing the murine signal peptide, the human extracellular domain and the murine transmembrane and cytoplasmic domains (designed and created by Genoway Lyon, France). This chimeric protein is expressed under the control of the FcγRIIb mouse endogenous promoter, keeping the endogenous mouse 5' and 3' untranslated regions intact. An FRT-flanked neomycin cassette was inserted in intron 3. Briefly, the targeting vector was transfected into C57BL/6 ES cells and recombined ES cell clones were them microinjected into blastocysts to give rise to male chimeras with a significant ES cell contribution. Breeding was established with C57BL/6 mice expressing the Flp-recombinase to produce the FcγRIIb humanized heterozygous line devoid of the neomycin cassette. Heterozygous 2K-KIX mice were interbred to produce the homozygous 2B-KIX; animal genotyping was performed by PCR, and a sample of each offspring was further confirmed by Southern blot.

HIV pseudovirus production:

pNLCH5.1 pseudotyped with HXB2 Env was produced by co-transfecting human embryonic kidney (HEK) 293T cells (NIH, AIDS Reagent Programme, Catalogue No: 103) with pNLCH5.1 (NL4–3-derived, Δenv, firefly luciferase inserted into nef open reading frame(26, 27) and the Env expression vector HXB2 (pHXB2 - NIH AIDS Reagent Programme, Catalogue No. 1069) in a 1:1 ratio using GENEFECT™ (Alkali Scientific Inc) according to the manufacturer's instructions. Transfected cells were incubated at 37°C in 5% CO2, and after 48h, supernatant was collected and centrifuged at 400 × g for 5 minutes and stored at −80°C for further use. Pseudovirus concentration was determined with a HIV p24 Antigen ELISA kit, according to the manufacturer's instructions (ZeptoMetrix).

Plasmids:

The pGag-EGFP plasmid (NIHARP cat #11468) used to prepare HIV, which directs Rev-independent expression of HIV Gag-EGFP fusion protein to form HIV, was obtained from Dr. Marilyn Resh through the NIH AIDS Reagent Program, Division of AIDS, NIAID, NIH. The pGag-EGFP plasmid was constructed by cloning Gag from pCMV55M1–10(28) into the pEGFP-N1 plasmid (Clontech)(29). Plasmid DNA was amplified in Escherichia coli DH5α; DH5α-containing pGag plasmid was grown in LB medium supplemented with 25 μg/mL kanamycin. The pHXB2 Env plasmid (NIHARP cat#1069), containing HXB2 gp160 under an SV40 promoter, was obtained from Dr. Kathleen Page and Dr. Dan Littman through the NIH AIDS Reagent Program, Division of AIDS, NIAID, NIH. Plasmid DNA was amplified in Escherichia coli DH5α; DH5α-containing pHXB2 Env plasmid was grown in LB medium supplemented with 50 μg/mL ampicillin. Plasmid purification used the BenchPro 2100 Plasmid Purification System (Invitrogen).

Preparation of HIV virus-like particles (HIV-LP) expressing HXB2 Env:

HIVs were produced in human embryonic kidney, 293T, cells (ATCC) and prepared as we described before (16). Cells were maintained in Dulbecco's Modified Eagle medium with 10% Fetal Bovine Serum. HIV expressing HXB2 Env were produced by transient transfection of HEK 293T cells with pGag-EGFP and pHXB2 Env using Lipofectamine 2000 transfection reagent (Life Technologies). 10^7 cells in T175 flasks were transfected with 30 μg HXB2 Env, 60 μg pGag-EGFP, and 360 μL Lipofectamine 2000 transfection reagent in serum/antibiotic-free medium. After 3–4 hours of incubation at 37°C the culture medium was replaced with DMEM + 10% FBS. HIV-containing supernatant was collected 72 hours after transfection and clarified by centrifugation at 2000 *x* g for 10 minutes. Clarified supernatant was further purified of cellular debris by 0.45 μm filtration, followed by ultracentrifugation through a 20% sucrose pad at 122000 *x* g for 2 hours at 4°C. The pellet was resuspended in filtered PBS.

Immunofluorescence and Immunoblotting.

Liver pieces of ~5mm in length were fixed in 4% paraformaldehyde-PBS for 2 hours at room temperature, washed with PBS (with 0.02% sodium azide) and infused in 20% sucrose-PBS overnight at 4°C. For immunofluorescence, cryostat sections of 5μm thickness were blocked with 5% milk in PBS, followed by incubation with primary Abs overnight. After 3 washes with PBS for one hour, sections were then incubated with fluorescently tagged secondary Ab for another hour at room temperature, then nuclei were stained with DAPI (100ng/ml) for 10 min. Sections were then mounted with Prolong Gold (Invitrogen) under coverslips. Control Abs refer to the list of isotype Abs with their respective secondary Ab. The images were obtained using an Olympus FluoView 1000 Laser Scanning Confocal microscope equipped with a spectral detection system for a finer separation of fluorochromes (FV 1000 spectra) along with 60X oil immersion lens at room temperature. Images were analyzed using ImageJ software (30)

Preparation of mouse LSEC.

Mice were anaesthetized under Isoflurane anesthesia and euthanized by decapitation. By incision via midline, the portal vein was exposed; a catheter was inserted and then connected to the buffer systems at 37°C. A cut was made in the inferior vena cava for perfusion buffer outflow. The liver was perfused with perfusion buffer (3.55 M NaCl, 170 mM KCl, 240 mM Hepes pH 7.4) followed by perfusion buffer containing research grade Liberase™ at a concentration of 5 mg/ml (Sigma). The digested liver was excised and Glisson's capsule was removed to release the cells into perfusion buffer containing 1% BSA. After filtering the cells, the cell suspension was centrifuged at 65g three times, to remove hepatocytes. The non-parenchymal cells (NPC) were pelleted from the supernatant and subjected to immuno-magnetic separation.

Highly purified LSEC were prepared from NPC using a triple selection method based on our data (Figure S1A) and also data from the literature that suggests that LSEC are $CD45^-$, $F4/80^-$, and $CD146^+$ cells, but KC are $CD45^+$ and $F4/80^+$ (15, 31, 32). Briefly, the F4/80– ve NPC were subjected to a second negative selection using anti-CD45 conjugated immunomagnetic bead and a positive selection using CD146 conjugated beads. For every

selection procedure, the cells from the previous procedure were suspended in MACS buffer and incubated with appropriate Ab-conjugated beads from Miltenyi Biotec and passed through MiniMacs magnetic columns. The purity of the LSEC was further confirmed by flow cytometry using markers for various cells in the liver, using the flow cytometry protocol below.

Flow cytometric analysis.

Five-color/two color flow cytometry analyses were done using a BD FACS Aria III flow cytometer equipped with four spatially separated beam spots (The laser wavelengths are 488 nm, 633 nm, 561 nm, 445 nm and 375 nm). Five Abs against various cells in the liver, each with distinctive and non-overlapping excitation wavelength were chosen and incubated with cells, i.e. 2.4G2 PE-Cy7 (LSEC marker), F4/80 PE (KC marker), NK-1.1 FITC(NK cell marker), Desmin Pac-blue (Stellate cell marker), Cd11c Percp (dendritic cell marker), and isotype controls IgG2b.κ PE-Cy7, IgG2a.κ PE, IgG2a.κ FITC, anti-Rab 405, American Hamster IgG Percp were used. Spectra of five Abs were assessed using Fluorescence SpectraViewer (Thermofisher) to confirm there was no spectra overlap. The data analysis was done using FlowJo software. To offset spectral overlap, compensations were done by subtracting unwanted signals using single and double stained control samples. The quadrant markers were set based on the isotype controls. For each analysis 10,000 events were analyzed.

Quantification of HIV p24.

The HIV p24 concentration was measured as pictograms per milliliter (pg/mL) using the commercially available Zeptometrix p24 ELISA kit. To determine HIV concentration as molecules of HIV/mL, a ratio of p24 concentration (pg/mL) to Nanoparticle Tracking Analysis (NTA; HIV/mL) was calculated for each HIV preparation. NTA was performed using Nanosight NS300 (Malvern) as elaborated earlier(16). HIVIG demonstrated concentration-dependent Anti-p24 blocking; a range of HIVIG concentration standards were used to correct all samples collected from mice injected with HIV-HIVIG.

Preparation of immune complexes.

All immune complexes (IC) were made prior to infusion into mice, and the size of IC particles were measured by NTA using Nanosight NS300 (Malvern) as elaborated earlier (16). Briefly, 5×10^{10} HIV was incubated with anti-HIV Abs at a concentration of either 25mg or 50mg/kg per mice for 4 hours at 37C. Two different anti-HIV Abs were used. The first, Human Immunodeficiency Virus immune globulin (HIVIG; NIHARP cat# 3957) pooled from plasma of asymptomatic, HIV Ab-positive donors with CD4+ counts above 400/μL. HIVIG was obtained from Dr Luiz Barbosa through NIH AIDS Reagent Program (33). Human IgG (Sigma-Aldrich) was used for control mice in all HIVIG studies. The second anti-HIV Ab preparation consisted of five monoclonal broadly neutralizing Abs (PGT 151, b12, PGT 121, PG 9 and 2F5). The control mice received Ab-free HIV infusions.

Clearance of HIV from bloodstream.

2B-KIX mice that were age and sex matched (Male and 12 weeks old) were infused via retro-orbital plexus with Ab-HIV or control Ab opsonized HIV. Blood samples were collected from the left retro-orbital plexus at 30 seconds, 2, 3, 5, and 10 minutes using heparinized capillary tubes. The 10 minute interval reflected near-maximum clearance uncomplicated by subsequent processes. Blood obtained at each time point was diluted. The standards were diluted in blood, similar to samples and the HIV p24 concentration was determined as pg/mL using p24 ELISA (Zeptometrix). No signs of anaphylaxis were noted during the short duration of the experiments.

In vivo analysis of HIV clearance.

The amounts of HIV in the whole blood were calculated using the HIV p24 concentrations and the blood volume of the mouse (2.58 mL/25g mouse(15)), and clearance were plotted as the amounts of HIV p24 per mouse versus time.

HIV pseudovirus-antibody binding assay.

The 96-well plates were coated with 10μg of Galanthus nivalis lectin (GNA) (34, 35) (Sigma-Aldrich) at a concentration of 0.1mg/ml and incubated overnight at RT. After washing with PBS, 10^{10} HIV in 10% goat serum was added to each well and incubated in 37°C for 30 minutes. To achieve maximum binding, the plates were centrifuged twice at 4000x G for 15 minutes at 25°C followed by 1h incubation at 37°C. After washing with PBS containing 10% goat serum, the Alexa 594 fluor-labelled HIVIG/Pentamix were added to the wells and incubated for 4 hours at 37°C. Controls included HIV alone and Abs alone. After washing with PBS containing 10% goat serum the concentration of HIV-GFP and Abs −594 was measured using Enspire™ Multimode Plate Reader (Perkin Elmer).

Labeling of antibodies and HIV.

The HIV or Abs at a concentration of 2mg/ml in 1X borate buffer (Thermo fisher) was incubated with 500μg/mL Alexa Fluor 488/Alexa Fluor 594 NHS Ester (Succinimidyl Ester) (Invitrogen) or FITC (Life science) for 2 hours at room temperature. The free dyes were then removed by dialysis against PBS overnight in Slide-A-lyzer dialysis kit (Life Science). The efficiency of conjugation was assessed by comparing the protein concentration (μg/μL) of the dialyzed Abs or HIV with the concentration of fluor (pmol/μL). The fluor concentration was converted to μg/μl using the formula weight; the dye-to-protein ratio of fluor-conjugated HIV was 1:40, the dye to protein ratio of fluor-conjugated Abs was 1:100.

Organ distribution of immune complex.

The immune complexes containing HIV HIV plus HIVIG-594 were prepared and infused into 2B-KIX mice via retro-orbital plexus for 10 minutes. The major organs, namely liver, heart, lung, spleen and kidney, were harvested after euthanizing the mice. Approximately 100mg of each organ was lysed in tissue cell lysis buffer (36) and fluorescence intensity was determined using an EnspireTM multimode plate reader (Perkin Elmer). The percentage distribution of HIVIG-594 was calculated by factoring the total weight of each organ.

In vivo localization of immune complex.

The immune complex containing HIV-488 plus HIVIG-594 was prepared and infused into 2B-KIX mice via retro-orbital plexus. After 3 min, the liver was harvested and fixed in 4% PFA. The liver samples were processed for immunofluorescence as we described earlier (15). The four-color immunofluorescence images were obtained via Olympus confocal microscope

Intracellular Localization of Immune Complex.

LSEC from 2B-KIX mice were plated on collagen-coated coverslips by incubating the cells for 2 hours in RMPI media containing 10% FBS in 24-well plates and washed twice with the same media to remove debris. The HIVIG-594 plus HIV-488 IC was then incubated with LSEC cells for 30 minutes at 37°C and 4°C respectively. Cells were washed to remove excess immune complex and fixed with 4% PFA. Nuclei were stained with DAPI. Cover slips containing LSEC were observed using Olympus Spectral FV1000 confocal microscopy

Endocytosis assay using live cell confocal microscopy.

LSEC isolated form 2B-KIX liver were seeded to collagen-coated dishes for 2h in RMPI media containing 10% FBS and then washed twice to remove debris. The HIV plus HIVIG-FITC immune complex was then incubated with LSEC cells for 3, 7, 10, 15 and 30 minutes at 37°C/ 4°C and washed twice with 4°C RPMI media without FBS. Cells were analyzed using Nikon A1R live cell confocal microscopy for imaging with plan Apo optics of 60x in oil, laser wavelength at 487.8nm, laser power 1.0, pinhole radius at 28.1μm, calibration of 0.21μm/px. The membrane-associated HIVIG-FITC was then quenched with 4mg/ml trypan blue (sigma) in PBS. Fluorescence images after quenching of trypan blue were obtained at the same spot. The images were quantified by ImageJ.

Penta-HIV immune complex colocalization to lysosomes of LSEC.

HIV-Penta mix in pH 8.5 borate buffer were labeled with Alexa 488 and Alexa 647, respectively. The free fluor was removed by dialysis against PBS. Immune complexes (ICs) were prepared by pre incubating 488-HIV and 647-Penta mix at 37°C for 4 hours. LSEC from 2B-KIX liver were plated on gelatin coated coverslip for 2 hours in DMEM/F12 media. 488-HIV-647-Penta immune complex were pulse chased by incubating with LSEC for 1.5 hours at 37°C then wash to remove unbound and incubated from 4 hours to 12 hours and fixed in 4% paraformaldehyde (PFA). LSEC were permeablized using ice cold methanol, blocked with human-IgG in PBS-FACS buffer at a concentration of 2mg/ml. LSEC were immuno-labelled with rat anti-mouse LAMP-1 Ab and followed by secondary 594-anti rat IgG. Nucleus was stained with DAPI. The over slips containing LSEC were analyzed and imaged in Olympus Spectral FV1000 Confocal microscopy. Lysosomal uptake percentage of ICs was calculated using ImageJ.

For colocalization of HIV-Penta immune complex with Texas Red dextran, LSEC from 2B-KIX mice were plated on gelatin coated coverslip for 2 hours. 488-HIV-647-Penta ICs and Texas Red-dextran were pulse chased by incubating with LSEC for 1.5 hours at 37°C and cells were washed to remove excessive IC, and incubated for overnight, and then fixed with

4% PFA. Nucleus was stained with DAPI. LSEC were then analyzed and imaged in Olympus Spectral FV1000 Confocal microscopy.

Scanning Electron Microscopy LSEC.

LSECs isolated from 2B-KIX mice were seeded to collagen coated dishes for 2 hours in RPMI media containing 10% FBS and then washed thrice with RPMI (10% FBS) to remove debris. The LSECs were then fixed with 2.5% glutaraldehyde in 0.1M phosphate buffer for 1 hours in RT, followed by 2 hours at 4°C. LSECs were post-fixed in 1% osmium in 0.1M Na cacodylate for 1hour. While rocking, cells were dehydrated 10min at a time in graded ethanol series (50%, 70%, 80%, 90%, 100%, 100%, 100% EtOH). All samples were then infiltrated with HMDS (hexamethyldisilazane) 15min at a time in a graded series (3:1 EtOH: HMDS, 1:1 EtOH: HMDS, 1:3 EtOH: HMDS, 100% HMDS, 100% HMDS, 100% HMDS). HMDS was removed from samples; samples were air dried and then mounted for imaging.

HIV pseudovirus Neutralization Assay.

Neutralization assay was performed using TZM-bl cells and HIV pseudotyped with HXB2 Env. Serial dilutions of HIVIG and pentamix of MAbs with a starting concentration of 5.9 and 6.6 mg/ml, respectively were made in DMEM medium in 96 well microtiter plate and isolated HXB2 virus at an approximate concentration of 1E8 was added to desired wells. The mixture was co-incubated for 2 h at 37°C including no Ab virus control and cells alone control in defined wells. After 2 h, immune complexes were added to target cells (1×10^4 TZM-bl) and incubated for 48h. HIV replication was assessed using quantitative Promega luciferase reporter assay kit. The average relative light units (RLU) were measured using Molecular Devices spectramax i3X injector. The relationship between HIV input and RLU was used to calculate the percentage of neutralization and also the median tissue culture infective dose that produces pathological changes in 50% of cell cultures infected (TCID50).

Statistical Analysis.

For statistical analysis a two-tailed Student's *t*-test was used for two-group comparison, and p value less than 0.05 was considered significant (*$p<0.05$, **$p<0.01$, ***$p<0.001$). All analyses were run using GraphPad Prism version 6 or SigmaPlot version 12.3.

Data availability.

All data in this article are available upon request. Information regarding human samples, experimental design, and materials can be found in the Materials and Methods section.

RESULTS:

Human LSEC express only FcγRIIb.

To determine the expression pattern in human liver for various FcγRs, we analyzed human liver by immunofluorescence microscopy (IF), using pan-anti-human FcγRII mAb KB61, which was demonstrated to have similar binding affinity to FcγRIIa and FcγRIIb (37). We confirmed the published finding that human liver sinusoidal endothelium is highly positive for FcγRII a/b expression (38). We further found that the IF signal from KB61 colocalizes

with an LSEC marker anti-mannose receptor (MR) (Figure 1 top row) showing a similar staining pattern. The MR expression in KC was confirmed to be weak or nil in human liver (data not shown) similar to murine liver (15). Importantly, we found that FcγRIIa/b expression colocalizes perfectly with the signal from anti-human FcγRIIb-specific pAb 163 (Figure 1, 2nd row) suggesting that LSEC specifically expresses FcγRIIb. In contrast, the anti-FcRγ-chain Ab does not stain FcγRIIa/b-positive endothelial cells (Figure 1, 3rd row); instead, the staining pattern of anti-FcRγ matches the KC-specific endosomal/lysosomal marker anti-CD68 (Figure 1, 4th row). Further colocalization analysis using antibodies against anti-human FcγRI and FcγRIII shows that FcγRI and FcγRIII, are not expressed in LSEC whereas they are in KC (Figure 1, bottom 2 rows). Using polyclonal antibodies (pAbs) specific for FcγRIIa and FcγRIIb, namely 260 and rabbit-anti FcγRIIb (Novus Biologicals) respectively, in an immunoblot protocol, we found that the human liver weakly expresses FcγRIIa (Figure 2B) compared to the positive control cell line U937. In contrast, human liver strongly expresses FcγRIIb (Figure 2A) similar to the positive Raji cell control. Reprobing the FcγR blots with anti-β-actin confirmed equal loading of samples (Figure 2 A and B, bottom panels). Together, these findings show that in human, LSEC express only FcγRIIb.

Construction of human FcγRIIb-expressing 2B-KIX mice and evaluation of transgene expression.

To evaluate human anti-HIV Abs in mice, we engineered a mouse strain expressing human rather than mouse FcγRIIb (2B-KIX: FcγRIIb-Knock-In; Xencor). Briefly, the gene sequence for the extracellular domain of mouse FcγRIIb (exon 4-exon7) was replaced with the gene sequence for the extracellular domain of human FcγRIIb; the sequence for the mouse intracellular domain was retained (Manuscript in review).

LSEC of 2B-KIX mice express human, but not mouse FcγRIIb.

To obtain purified LSEC preparations we avoided controversies regarding the LSEC phenotype shown differently by various laboratories (18). Instead, we developed our own method employing two additional negative selection steps, using mAb F4/80 and anti-CD45 mAb, to remove Kupffer cells (KC) and other leukocytes, respectively from liver cell suspensions. The histogram analysis of purified and enriched LSEC ($F4/80^{-}CD45^{-}CD146^{+}$) from BALB/c mice using two-color flow cytometry confirmed the presence of LSEC marker in purified cells that were seen earlier *in vivo*, namely $2.4G2^{+}$ and $F4/80^{-}$(15) (Figure 3A). The purity of immuno-magnetically triple-selected LSEC was reproducibly >97% and the yield was 2 million LSEC per mouse (n=9). The gating strategy before and after enrichment of LSEC and the positive and negative selection methods are validated based on enrichment of LSEC achieved from 3% of non-parenchymal cells to 88% (Figure S1 B). The five-color flow cytometric analysis using markers for various liver cells, namely F4/80 (KC), CD11c (dendritic cells), NK 1.1(NK cells), desmin (stellate cells), and 2.4G2 (LSEC), substantiated the purity of the LSEC preparation, in that we found <1% contamination with other liver cells (Figure 3B). The presence of fenestrae are considered the gold standard morphologic feature distinguishing LSEC from other cells of the liver (39). LSEC purified by triple immune-magnetic separation showed by SEM the typical fenestrae in the membrane (Figure 3C).

In order to test the phenotype of purified LSEC from humanized mice, we first confirmed the specificity of anti-human FcγRIIb mAb 4F5 (25) labeled with fluor Alexa 594, for specificity for human, but not mouse, FcγRIIb, using mouse B cell line (A20), a human B cell line (Raji), and a cell line that lacks FcγR (HEK) (Figure S1 C–E). The two-color flow cytometry and confocal imaging of 2B-KIX LSEC showing positivity for 4F5 and negativity for 2.4G2 confirms that the extracellular domain of LSEC from 2B-KIX expresses human FcγRIIb (4F5) and lacks the extracellular domain of mouse FcγRIIb (2.4G2) (Figure 3D) (Figure 3E). On the other hand, LSEC from BALB/c mice did not bind to anti-human FcγRIIb mAb 4F5, but bound to 2.4G2 (Figure S2). LSEC from 2B-KIX mice consistently expressed the characteristic fenestrae of the LSEC phenotype. EM images of purified LSEC mounted from cell suspensions showed spheres with redundant folded plasma membrane, consistent with their appearance *in vivo* as extended thin cells (Figure 3F).

NAbs enhance clearance of HIV from circulation better than HIVIG.

Having earlier noted that intravenously infused HIV-LP are cleared from circulation largely by LSEC (16), we asked whether such clearance could be enhanced with anti-HIV polyclonal Abs (pAbs) and monoclonal NAbs. In order to study Ab-mediated enhancement of clearance, we first prepared Ab-HIV-LP and measured the particle size by nanosight. The diameters of the particles, measured as mode ± SE by high-resolution image analysis of particle Brownian motion were, for HIV-LP alone, ~120 ± 7 nm; for HIV-LP opsonized with anti-HIV pAbs (HIVIG-HIV-LP), ~143± 10 nm; and for HIV-LP opsonized with a mixture of 5 NAbs (penta-HIV-LP), ~134 ± 8 nm. Larger size of the HIVIG-HIV-LP could be because HIVIG contain both NAbs and non-NAbs that can recognize a wide variety of Env epitopes, including non-functional spike proteins. In contrast, NAbs recognize only 5 epitopes on native Env trimers, each with a maximal occupancy of 3 antibodies per specificity. Our data are in accordance with *in vitro* virion capture assays where bNAbs usually perform less well compared to non-NAbs contained in HIVIG (40–43). We then infused 2B-KIX mice intravenously with either HIVIG-HIV-LP or penta-HIV-LP along with their respective controls, and measured the disappearance of HIV-LP from circulation over time. The HIV-LP concentrations in blood were measured using a p24 ELISA. The standards were also diluted with blood. Blood HIV-LP concentrations were not significantly different at early times between HIVIG and human IgG, but became significantly lower in HIVIG compared to human IgG at later time points, i.e., 5 and 10 min (Figure 4A). In contrast, Blood HIV-LP concentrations were significantly lower at all-time points when treated with pentamix of 5 NAbs compared to irrelevant isotype control anti-dengue antibody (Figure 4B). Interestingly, though the shape of clearance curves of HIV-LP appears very similar between anti-dengue-HIV-LP and penta-HIV-LP, the major drop of blood HIV levels occurs in 30 seconds after infusion, suggesting a very rapid and huge clearance by penta-HIV-LP within 30 seconds. With one-pass circulation time of blood in a mouse being approximately 15 seconds in circulation (44), the HIV-LP was exposed to LSEC with 2 passes, during which NAbs have facilitated clearance of HIV-LP. In order to quantitatively compare the difference in clearance between HIVIG and Penta, we subtracted the amount of HIV-LP remaining in blood of antibody-treated groups from that of their respective controls at the end of the clearance (10 min) and plotted in Figure 4C. The data suggests that NAbs clears HIV-LP significantly more than HIVIG.

We next asked whether the enhanced clearance by NAbs was due to more amount of Abs bound to HIV-LP. We plated fixed amounts of HIV-LP, added varying concentrations of Abs, quantified Ab binding, and plotted the ratio of Ab to HIV-LP vs the concentration of Ab. The binding curve suggested that the saturating concentration at which maximum binding occurs was not different between HIVIG and pentamix (Figure 4D), both saturating at about 0.5mg/ml after which no further binding occurred. However, at every input concentration about twice as much HIVIG was bound to HIV-LP than with pentamix.

Relating binding and clearance, we observed lower binding *in vitro* and enhanced clearance of HIV-LP *in vivo* by pentamix compared to HIVIG. Our results suggests that HIVIG may dissociate from HIV-LP *in vivo* where as pentamix did not. We further confirmed that pentamix has higher neutralization potential than does HIVIG using pseudotyped HIV (Figure 4E).

Liver is the major organ that clears antibody-opsonized HIV-LP.

To identify the organ responsible for the enhanced clearance of Ab-HIV-LP, we quantified the organ distribution of intravenously infused mixtures of HIVIG and Alexa 594 conjugated-HIV-LP (594-HIV-LP) following our published protocols (10, 15). Ten minutes after infusions, we recovered 86±9% in liver, 2.2±1.1% in lung, 0.1±0.3% in spleen, 1.8±1.3% in kidney and 9.0±9% in blood circulation suggesting strongly that liver is the major organ responsible for clearing circulating Ab-opsonized HIV-LP (Figure 5A).

In the liver, HIVIG-HIV immune complex is distributed primarily to LSEC.

Having confirmed that the liver is the major organ clearing HIVIG-HIV-LP, we elucidated the cell types responsible for the rapid uptake. We examined paraformaldehyde (PFA)-fixed liver sections by 4 color fluorescence confocal microscopy at three minutes post infusion. To visualize the immune complex we tagged HIV-LP with Alexa 488 fluor (green) and HIVIG with Alexa 594 fluor (red). Abundant green puncta colocalizing with red puncta lined the sinusoids of liver images, indicating close proximity and distribution of complexes of HIVIG 594 - HIV-LP 488 (Figure 5B). No HIV-LP or Ab was associated with hepatocytes or with the endothelial cells of larger veins. Quantification from more than 30 similar liver images from three different mice revealed that a remarkably large amount of immune complex (about ~70% of HIV-LP 488 and 78% of HIVIG 594) localized to LSEC, confirming that LSEC are the major cells responsible for the clearance of HIVIG-HIV-LP circulating immune complexes (Figure 5C).

Human FcγRIIb mediates clearance of HIVIG-opsonized HIV-LP.

Having learned that LSEC are the major cell involved in clearing HIVIG-HIV-LP (Figure 5) and that LSEC from 2B-KIX mice exclusively express human FcγRIIb (Figure 3), we investigated whether human FcγRIIb mediates the enhanced clearance of HIVIG-HIV-LP. To address this question, HIVIG-HIV-LP was infused into both 2B-KIX mice and FcγRIIb KO mice, and decay curves were plotted. As predicted, blood HIV-LP concentrations decreased significantly more slowly in FcγRIIb KO mice than in 2B-KIX mice (Figure 6).

LSEC bind and endocytose HIVIG-HIV-LP immune complexes.

After demonstrating that HIVIG-HIV-LP complexes are eliminated from blood by liver LSEC FcγRIIb (Figure 5B & 5C), we identified the effector mechanism by which HIVIG-HIV-LP was taken up by LSEC. LSEC from 2B-KIX mice were used to study the immune complex *in vitro* uptake process in a time dependent manner at 37°C and 4°C. In confocal images of LSEC from 2B-KIX mice, we found HIV-LP 488 (green puncta) colocalized with HIVIG 594 (red puncta), confirming the association of the HIV-LP with HIVIG (Figure 7A). When incubated with LSEC at 37°C, HIVIG 594 -HIV-LP 488 appeared to move into LSEC during 30 min incubation (Figure 7B). In contrast, at 4°C, HIVIG 594 -HIV-LP 488 associated only with the LSEC outer membrane.

Quantifying the endocytosis (Figure 7B, C&D) using trypan blue as a quenching reagent of membrane associated FITC fluorescence confirmed that at 37°C, HIVIG plus FITC-HIV-LP bound increasingly to LSEC *in vitro* during the first 15 minutes and then plateaued from 15 to 30 minutes (45, 46), whereas mouse macrophage cell line RAW 264.7 starts to endocytose only at 10 minutes (Data not shown). The percentage of internalized immune complex increased from ~50% to ~75% during the 30 minutes incubation, extending our *in vivo* results (Figure 7C). At 4°C, the quantification showed no increase in uptake or internalization of HIVIG FITC-HIV to LSEC within 30 minutes (Figure 7D). These findings strongly suggest that the uptake and clearance of HIVIG FITC-HIV-LP by LSEC occurs via an endocytic mechanism.

Pentamix-HIV-LP immune complex localizes within lysosomes of LSEC.

Next, we investigated the fate of endocytosed Ab-HIV-LP. Since lysosomes function to degrade endocytosed biological proteins and particle, we asked whether Ab-HIV-LP could traffic to the lysosomes of LSEC. Anti-LAMP1 immunofluorescence staining for lysosome associated membrane protein (LAMP1) in LSEC shows that LSEC are in the process of endocytosing penta-HIV-LP within small vesicles in close proximity to the nucleus (Figure 8). In addition, all vesicles containing the penta-HIV-LP were LAMP1 positive.

We used a second strategy to confirm that penta-HIV-LP were endocytosed into endosomes that fuse with lysosomes. In this case, LSEC were incubated with Texas Red-dextran for 1.5 h followed by a chase for either 4.5 h or 10.5 h, leading to dextran localization to lysosomes (47). As expected, penta-HIV-LP co-localized with Texas Red-dextran within lysosomes at 6 and 12 h (Figure S3). Together, these results indicate that penta-HIV-LP are taken up into vesicles that fuse with lysosomes.

To establish the capacity of LSEC to clear circulating Ab-HIV-LP, we next used high magnification image analysis to measure the average volume and number of LAMP1-positive vesicles containing HIV-LP particles at the 12 h time point. Each LSEC contained 50 to 100 LAMP1-positive vesicles and ~70% of them were filled with Ab-HIV-LP. The average diameter of the vesicles was 1.1 μm, corresponding to an average volume of 0.69 μm^3. Given the average size of Ab-HIV-LP (0.14 μm in diameter and volume of 0.0014 μm^3), we calculated that each LAMP1-positive vesicle could accommodate up to ~492 Ab-

HIV-LP and one cell could ingest up to 25,000 Penta-HIV-LP. With a minimum of at least four million LSEC per mouse, LSEC could clear up to 10^{11} Penta-HIV-LP IC per mouse.

DISCUSSION:

Our findings presented here reveal several novel features on the mechanism of how anti-HIV Ab hastens the clearance of HIV-LP particles from the systemic blood circulation in mice. We demonstrate that intravenously infused HIV-LP opsonized with Ab is cleared from blood by FcγRIIb expressed on the surface of LSEC. Once cleared by LSEC, cell-bound HIV-LP is endocytosed. Previous reports have suggested that clearance of cell-associated HIV occurs by activation of FcγR (48, 49), mediated by effector functions such as ADCC and phagocytosis. Our results suggest that elimination of cell-free HIV by Abs occurs mainly via inhibitory receptor FcγRIIb. Previous reports of Ab-mediated acceleration of virus (50) and HIV (4) provided the initial stimulus for our studies. In this report, we extended these studies and identified the effector cell, effector function and Fcγ receptor as important components of the cell-free HIV clearance. Specifically, we show that un-opsonized HIV-LP are cleared from blood by a non-Fcγ receptor-mediated mechanism that has yet to be fully explored (16). Further, we show that both HIV-LP and Ab-HIV-LP, once cleared, eventually reach lysosomes inside LSEC, presumably for degradation. The Ab impact on HIV clearance is apparent from our composite experimental results.

The major difference between the control Ab opsonized HIV and Ab-HIV at the first measurement time point (Figure 4B) is typical of LSEC clearance mechanism that we have repeatedly observed for various ligands including small immune complexes and LPS (10) (Manuscript in review). We interpret these kinetics as first minute after infusion, the LSEC FcγRIIb become rapidly and maximally occupied by Ab-HIV, making majority of Ab-HIV to disappear from the circulation so quickly, after which only very slow decay happens. The control Ab opsonized HIV clearance may indicate the clearance of naïve HIV that we have reported earlier (16), which is further enhanced by the presence of anti-HIV antibodies (Figure 4). Our data suggest that the rapid clearance of Ab-HIV from blood circulation depicted in Figure 4, is followed by endocytosis uptake of immune complex (Figure 7), and further followed by trafficking to the lysosomes (Figure 8). Previous literature suggests that possible routes for HIV-1 infection include fusion at the cell surface and fusion early in the endocytic pathway prior to lysosomal acidification. In lysosomes the HIV are degraded by lysosomal acidification (51). Thus, although HIV-LP that enters the host cell can also cause productive infection, the majority of HIV-LP internalized by endocytosis and localized in a LAMP1 organelle are not productively infective and are eventually degraded. The fast kinetics of clearance followed by faster endocytosis and trafficking to lysosomes represent significant cellular host defense to HIV-LP by LSEC. Indeed, previous studies demonstrated that treatment of cells with pharmacological agents that elevate the pH of lysosomes allows $HIV\text{-}LP_{SF2}$ to efficiently infect host cells, suggesting that lysosomal uptake of HIV moves virions into a degradation pathway (52). The degradation pathway has been shown to extend to all HIV isolates tested regardless of co-receptor used for infection (51). We demonstrate in that no other organ or cell type exerted substantial endocytosis of HIV. Although we have used non-infectious HIV-LP to identify the effector cell involved in clearance, others have also shown that Ab-opsonized infectious HIV_{DH12} particles are rapidly degraded in the liver

of macaques, when they were unable to demonstrate the presence of HIV_{DH12} RNA (4). Thus, we speculate that, in human LSEC, FcγRIIb-mediated endocytosis of Ab-opsonized HIV leads to viral degradation into lysosomes faster than HIV alone, minimizing the likelihood of productive HIV infection.

We can effectively exclude the participation of other FcγR in the clearance process we describe, given that FcγRIIb is the only Fc family member expressed on LSEC of both mouse and human. Therefore, while FcγRIIb is commonly known for its capacity to inhibit agonist activity driven by other members of the FcγR family, and is thus dubbed the 'inhibitory' FcγR, it can also mediate endocytosis of IgG immune complexes, ordinarily considered an 'activating' or 'agonist' function, as shown in transfected cell lines (53–55). While the former inhibitory function requires a specific sequence in the cytoplasmic tail of the FcγRIIb protein centered about a phosphotyrosine, this unique tail sequence appears not to be required for the endocytic function (53, 54, 56).

Attempting to clarify the relationship of receptor affinity for IgG and the avidity of receptor-expressing cells for IgG-opsonized virus, we note that the avidity of an opsonized particle for an FcγR-expressing cell is a complex phenomenon. Two variables must be considered. One is the affinity of the Ab for the receptor, which varies among IgG subclasses up to ~50 fold, for the low affinity receptors (57, 58). The other is the number of Abs linking the particle with the FcγR-expressing cell that constitutes the avidity. The magnitude of the avidity depends on the sum of binding energies of the several Ab molecules mediating the virus-cell interaction. Previous studies showed that avidity (of a particle for a cell) increased about 300 fold when four Abs, rather than a single Ab molecule, bound to a particle (59–61). All the NAbs that we have used are IgG1 subclass. The binding affinities of human FcγRIIb for human IgG1, IgG3 and IgG4 are similar, the outlier being IgG2, which has very low affinity. Considering avidity, we anticipate that virtually all subclasses of IgG Ab, regardless of their individual affinities for FcγRIIb, would likely mediate an effective endocytic response.

Our results show that a mixture of NAbs clear HIV more efficiently from circulation than polyclonal HIVIG. Why do NAbs clear more vigorously than the HIVIG even though HIVIG offered a higher antigen to antibody ratio than NAbs? Possibly, HIVIG from non-symptomatic HIV patients consist of Abs against multiple epitopes in HIV in addition to irrelevant antibodies, leading to crosslinking *in vitro*, but the antibodies may be due to weaker affinity detach *in vivo* resulting in weaker clearance. Identifying a combination of NAb with very high binding affinity for HIV has the potential to form immune complexes of higher Ab to HIV ratios. This might enhance the clearance function of NAb, even at lower therapeutic concentrations. Moreover, our data suggest that NAb opsonized HIV or neutralized HIV do not remain in the circulation, but rather are actually eliminated from circulation. Our data also propose that polyclonal anti-HIV Abs, whether elicited by infection or by a vaccine, could accelerate viral clearance from circulation.

While we have not tested purified non-NAbs for their capacity to mediate HIV clearance in our assays by comparing neutralizing and non-neutralizing mAbs, we think it highly likely that clearance by HIVIG indicates mediation by both Ab classes as long as they maintain

affinity *in vivo*. Thus, our studies showing clearance of cell-free HIV complement the observations of others that these antibodies clear HIV-infected cells (49, 62, 63).

Our results show that a little-studied innate immune function, mediated by an Fcγ receptor in the liver, may contribute to the control of HIV infection. Such a control mechanism, whether elicited during HIV infection or by HIV vaccines, might not offer complete protection, given that the host ultimately succumbs, for a variety of reasons, including a higher production rate of HIV(14). However, we note that the clearance capacity of FcγRIIb can be enhanced by genetic manipulation of the NAb to have enhanced binding for FcγRIIb (en-FcγRIIb NAb). Such a strategy, currently exploited for treatment of systemic lupus erythematosus and other autoimmune diseases, involves modification of the Fc region of human IgG1 to enhance its affinity for FcγRIIb by 300–400 fold without increasing its affinity for FcγRI, FcγRIIa, or FcγRIIIa (64, 65). Thus, our project may provide a potential approach to enhance the efficacy of HIV Ab immunotherapy.

Furthermore, the en-FcγRIIb NAb therapy can be part of “shock and kill” approach to eliminate latest HIV reservoirs (66) that induces HIV production from reservoirs using latency reversing agents (LRA) and then eliminate HIV. But the elimination process has to be rapid, before HIV establish another reservoir elsewhere via systemic viremia (66). Our findings suggests that using LSEC FcγRIIb mediated endocytosis ability, the rapid clearance from blood stream can be achieved within few minutes. Accordingly, pairing LRA with en-FcγRIIb NAb might help to completely eradicate HIV from infected individuals.

Supplementary Material

Refer to Web version on PubMed Central for supplementary material.

ACKNOWLEDGMENT:

The authors are grateful to Dr. Sara Cole, Dr. Angela Blissett, Richard Montione, and Brian Kemmenoe at The Ohio State University Campus Microscopy and Imaging Facility for training with confocal imaging; to Bryan McElwain and Alex Cornwell at Analytical Cytometry, The Ohio State University for help with BD FACS Aria III Flow Cytometer; to Dr. Dan Birmingham for IgG purification of rabbit polyclonal Ab 163; to Dr. D. Mason at Radcliffe Hospital, Oxford, U.K), KB61 Ab; to Dr. Jessica Mates for preparation of pGAG-EGFP and prior HIV preparation design; Drs. Ozan Suer and Zhili Yao for the VLP preparations, VLP labeling and microscopy; Dr. Beth Schachter for editorial support in the preparation of manuscript; and Genoway (Lyon, France) and Charles River for generating and maintaining the human FcγRIIb expressing 2B-KIX mice. The reagent HIVIG was obtained through the NIH AIDS Reagent Program, Division of AIDS, NIAID, NIH: Anti-HIV Immune Globulin (HIVIG) from NABI and NHLBI (cat# 3957). The LAMP1 monoclonal Ab developed by J. Thomas August was obtained from the Developmental Studies Hybridoma Bank, created by the NICHD of the NIH and maintained at The University of Iowa, Department of Biology, Iowa City, IA 52242. [45]

Research reported in this publication was supported by the National Institute of Arthritis and Musculoskeletal and Skin Diseases of the National Institutes of Health under Award Number AR066330. The content is solely the responsibility of the authors and does not necessarily represent the official views of the National Institutes of Health.

References:

1. Marasco WA, and Sui J– 2007. The growth and potential of human antiviral monoclonal antibody therapeutics. Nat. Biotechnol 25: 1421–1434. [PubMed: 18066039]
2. Barouch DH, Whitney JB, Moldt B, Klein F, Oliveira TY, Liu J, Stephenson KE, Chang HW, Shekhar K, Gupta S, Nkolola JP, Seaman MS, Smith KM, Borducchi EN, Cabral C, Smith JY,

Blackmore S, Sanisetty S, Perry JR, Beck M, Lewis MG, Rinaldi W, Chakraborty AK, Poignard P, Nussenzweig MC, and Burton DR– 2013. Therapeutic efficacy of potent neutralizing HIV-1-specific monoclonal antibodies in SHIV-infected rhesus monkeys. Nature 503: 224–228. [PubMed: 24172905]

3. Hessel AJ, Hangartner L, Hunter M, Havaenith CEG, Beurskens FJ, Bakker JM, Lanigan CMS, Landucci G, Forthal DN, Parren PWHI, Marx PA, and Burton DR– 2007. Fc receptor but not complement binding is important in antibody protection against HIV. Nature 449: 101–105. [PubMed: 17805298]
4. Igarashi T, Brown C, Azadegan A, Haigwood N, Dimitrov D, Martin MA, and Shibata R– 1999. Human immunodeficiency virus type 1 neutralizing antibodies accelerate clearance of cell-free virions from blood plasma. Nat. Med 5: 211–216. [PubMed: 9930870]
5. Parsons MS, Lee WS, Kristensen AB, Amarasena T, Khoury G, Wheatley AK, Reynaldi A, Wines BD, Hogarth PM, Davenport MP, and Kent SJ– 2019. Fc-dependent functions are redundant to efficacy of anti-HIV antibody PGT121 in macaques. J Clin Invest 129: 182–191. [PubMed: 30475230]
6. Nimmerjahn F, and Ravetch JV– 2006. Fcγ receptors: Old friends and new family members. Immunity 24: 19–28. [PubMed: 16413920]
7. Hogarth PM 2002. Fc receptors are major mediators of antibody based inflammation in autoimmunity. Curr. Opin. Immunol 14: 798–802. [PubMed: 12413532]
8. Nimmerjahn F, and Ravetch JV– 2007. Fc-receptors as regulators of immunity. Adv Immunol 96: 179–204. [PubMed: 17981207]
9. Smith KGC, and Clatworthy MR– 2010. FcγRIIB in autoimmunity and infection: evolutionary and therapeutic implications. Nature Reviews Immunology 10: 328–342.
10. Ganesan LP, Kim J, Wu Y, Mohanty S, Phillips GS, Birmingham DJ, Robinson JM, and Anderson CL– 2012. FcgammaRIIb on Liver Sinusoidal Endothelium Clears Small Immune Complexes. J. Immunol 189: 4981–4988. [PubMed: 23053513]
11. Praaning-van Dalen DP, DeLeeuw DP, Brouwer AM, DeRuiter A, and Knook DL– 1982. Ultrastructural and biochemical characterization of endocytic mechanisms in rat liver kupffer and endothelial cells. In Proceedings of the Second International Kupffer Cell Symposium, held in Noordwijkerhout, the Netherlands, 29 August-2 September, 1982. 271–278.
12. Kamimoto M, Rung-Ruangkijkrai T, and Iwanaga T– 2005. Uptake ability of hepatic sinusoidal endothelial cells and enhancement by lipopolysaccharide. Biomed Res 26: 99–107. [PubMed: 16011302]
13. Zhang L, Dailey PJ, Gettie A, Blanchard J, and Ho DD– 2002. The liver is a major organ for clearing simian immunodeficiency virus in rhesus monkeys. J. Virol 76: 5271–5273. [PubMed: 11967341]
14. Perelson AS, Neumann AU, Markowitz M, Leonard JM, and Ho DD– 1996. HIV-1 Dynamics in Vivo: Virion Clearance Rate, Infected Cell Life-Span, and Viral Generation Time. Science 271: 1582–1586. [PubMed: 8599114]
15. Ganesan LP, Mohanty S, Kim J, Clark KR, Robinson JM, and Anderson CL– 2011. Rapid and Efficient Clearance of Blood-borne Virus by Liver Sinusoidal Endothelium. PLoS. Pathog 7: e1002281. [PubMed: 21980295]
16. Mates JM, Yao Z, Cheplowitz AM, Suer O, Phillips GS, Kwiek JJ, Rajaram MV, Kim J, Robinson JM, Ganesan LP, and Anderson CL– 2017. Mouse Liver Sinusoidal Endothelium Eliminates HIV-Like Particles from Blood at a Rate of 100 Million per Minute by a Second-Order Kinetic Process. Front Immunol 8: 35. [PubMed: 28167948]
17. Ganesan LP, Mates JM, Cheplowitz AM, Avila CL, Zimmerer JM, Yao Z, Maiseyeu A, Rajaram MV, Robinson JM, and Anderson CL– 2016. Scavenger receptor B1, the HDL receptor, is expressed abundantly in liver sinusoidal endothelial cells. Sci. Rep 6: 20646. [PubMed: 26865459]
18. Elvevold K, Smedsrod B, and Martinez I– 2008. The liver sinusoidal endothelial cell: a cell type of controversial and confusing identity. AJP - Gastrointestinal and Liver Physiology 294: G391–G400.
19. Sorensen KK, Simon-Santamaria J, McCuskey RS, and Smedsrod B– 2015. Liver Sinusoidal Endothelial Cells. Compr Physiol5:1751–1774, *2015* 5: 1751–1775. [PubMed: 26426467]

20. Zhu P, Liu J, Bess J Jr., Chertova E, Lifson JD, Grise H, Ofek GA, Taylor KA, and Roux KH– 2006. Distribution and three-dimensional structure of AIDS virus envelope spikes. Nature 441: 847–852. [PubMed: 16728975]
21. Zhu P, Chertova E, Bess J Jr., Lifson JD, Arthur LO, Liu J, Taylor KA, and Roux KH– 2003. Electron tomography analysis of envelope glycoprotein trimers on HIV and simian immunodeficiency virus virions. Proc. Natl. Acad. Sci. U. S. A 100: 15812–15817. [PubMed: 14668432]
22. Parren PW, and Burton DR– 2001. The antiviral activity of antibodies in vitro and in vivo. Adv. Immunol 77: 195–262. [PubMed: 11293117]
23. Burton DR 2002. Antibodies, viruses and vaccines. Nature Reviews Immunology 2: 706–713.
24. Huber M, and Trkola A– 2007. Humoral immunity to HIV-1: neutralization and beyond. J. Intern. Med 262: 5–25. [PubMed: 17598812]
25. Su K, Yang H, Li X, Li X, Gibson AW, Cafardi JM, Zhou T, Edberg JC, and Kimberly RP– 2007. Expression profile of FcgammaRIIb on leukocytes and its dysregulation in systemic lupus erythematosus. J. Immunol 178: 3272–3280. [PubMed: 17312177]
26. Garnsey MR, Matous JA, Kwiek JJ, and Coltart DM– 2011. Asymmetric total synthesis of (+)- and (−)-clusianone and (+)- and (−)-clusianone methyl enol ether via ACC alkylation and evaluation of their anti-HIV activity. Bioorg. Med. Chem. Lett 21: 2406–2409. [PubMed: 21414776]
27. RUSSELL ES, Kwiek JJ, Keys J, Barton K, Mwapasa V, Montefiori DC, Meshnick SR, and Swanstrom R– 2011. The genetic bottleneck in vertical transmission of subtype C HIV-1 is not driven by selection of especially neutralization-resistant virus from the maternal viral population. J. Virol 85: 8253–8262. [PubMed: 21593171]
28. Schwartz S, Campbell M, Nasioulas G, Harrison J, Felber BK, and Pavlakis GN– 1992. Mutational inactivation of an inhibitory sequence in human immunodeficiency virus type 1 results in Rev-independent gag expression. J. Virol 66: 7176–7182. [PubMed: 1433510]
29. Hermida-Matsumoto L, and Resh MD– 2000. Localization of human immunodeficiency virus type 1 Gag and Env at the plasma membrane by confocal imaging. J. Virol 74: 8670–8679. [PubMed: 10954568]
30. Yao Z, Mates JM, Cheplowitz AM, Hammer LP, Maiseyeu A, Phillips GS, Wewers MD, Rajaram MV, Robinson JM, Anderson CL, and Ganesan LP– 2016. Blood-Borne Lipopolysaccharide Is Rapidly Eliminated by Liver Sinusoidal Endothelial Cells via High-Density Lipoprotein. J. Immunol 197: 2390–2399. [PubMed: 27534554]
31. Hegenbarth S, Klugewitz K, Hamann A, Diehl L, and Knolle P– 2006. Efficient isolation of liver sinusoidal endothelial cells (LSECs) by immunomagnetic separation. MACS&more 10: 8–10.
32. Katz SC, Pillarisetty VG, Bleier JI, Shah AB, and Dematteo RP– 2004. Liver sinusoidal endothelial cells are insufficient to activate T cells. J. Immunol 173: 230–235. [PubMed: 15210779]
33. Cummins LM, Weinhold KJ, Matthews TJ, Langlois AJ, Perno CF, Condie RM, and Allain JP– 1991. Preparation and characterization of an intravenous solution of IgG from human immunodeficiency virus-seropositive donors. Blood 77: 1111–1117. [PubMed: 1995097]
34. Sourial S, Warnmark A, Nilsson C, Bjorling E, Achour A, and Harris RA– 2005. Cloning, expression, and purification of HIV-2 gp125: A target for HIV vaccination. Mol. Biotechnol 30: 155–162. [PubMed: 15920286]
35. Gilljam G 1993. Envelope glycoproteins of HIV-1, HIV-2, and SIV purified with Galanthus nivalis agglutinin induce strong immune responses. Aids Res. Hum. Retroviruses 9: 431–438. [PubMed: 8318269]
36. Lyden TW, Robinson JM, Tridandapani S, Teillaud JL, Garber SA, Osborne JM, Frey J, Budde P, and Anderson CL– 2001. The Fc receptor for IgG expressed in the villus endothelium of human placenta is Fcγ RIIb2. J. Immunol 166: 3882–3889. [PubMed: 11238632]
37. Veri MC, Gorlatov S, Li H, Burke S, Johnson S, Stavenhagen J, Stein KE, Bonvini E, and Koenig S– 2007. Monoclonal antibodies capable of discriminating the human inhibitory Fcgamma-receptor IIB (CD32B) from the activating Fcgamma-receptor IIA (CD32A): biochemical, biological and functional characterization. Immunology 121: 392–404. [PubMed: 17386079]

38. Pulford K, Ralfkiaer E, Macdonald SM, Erber WN, Falini B, Gatter KC, and Mason DY– 1986. A new monoclonal antibody (KB61) recognizing a novel antigen which is selectively expressed on a subpopulation of human B lymphocytes. Immunol 57: 71–76.
39. Braet F, and Wisse E– 2002. Structural and functional aspects of liver sinusoidal endothelial cell fenestrae: a review. Comparative Hepatology 1: 1–17. [PubMed: 12437787]
40. Nyambi PN, Mbah HA, Burda S, Williams C, Gorny MK, Nadas A, and Zolla-Pazner S– 2000. Conserved and exposed epitopes on intact, native, primary human immunodeficiency virus type 1 virions of group M. J. Virol 74: 7096–7107. [PubMed: 10888650]
41. Moore PL, Crooks ET, Porter L, Zhu P, Cayanan CS, Grise H, Corcoran P, Zwick MB, Franti M, Morris L, Roux KH, Burton DR, and Binley JM– 2006. Nature of nonfunctional envelope proteins on the surface of human immunodeficiency virus type 1. J Virol 80: 2515–2528. [PubMed: 16474158]
42. Poignard P, Moulard M, Golez E, Vivona V, Franti M, Venturini S, Wang M, Parren PW, and Burton DR– 2003. Heterogeneity of envelope molecules expressed on primary human immunodeficiency virus type 1 particles as probed by the binding of neutralizing and nonneutralizing antibodies. J. Virol 77: 353–365. [PubMed: 12477840]
43. Liu Y, Pan J, Cai Y, Grigorieff N, Harrison SC, and Chen B– 2017. Conformational States of a Soluble, Uncleaved HIV-1 Envelope Trimer. *J. Virol* 91.
44. Debbage PL, Griebel J, Ried M, Gneiting T, DeVries A, and Hutzler P– 1998. Lectin intravital perfusion studies in tumor-bearing mice: micrometer-resolution, wide-area mapping of microvascular labeling, distinguishing efficiently and inefficiently perfused microregions in the tumor. J. Histochem. Cytochem 46: 627–639. [PubMed: 9562571]
45. Sahlin S, Hed J, and Rundquist I– 1983. Differentiation between attached and ingested immune complexes by a fluorescence quenching cytofluorometric assay. J Immunol. Methods 60: 115–124. [PubMed: 6406600]
46. Schuurhuis DH, Ioan-Facsinay A, Nagelkerken B, van Schip JJ, Sedlik C, Melief CJ, Verbeek JS, and Ossendorp F– 2002. Antigen-antibody immune complexes empower dendritic cells to efficiently prime specific CD8+ CTL responses in vivo. J Immunol 168: 2240–2246. [PubMed: 11859111]
47. Johnson DE, Ostrowski P, Jaumouille V, and Grinstein S– 2016. The position of lysosomes within the cell determines their luminal pH. J Cell Biol 212: 677–692. [PubMed: 26975849]
48. Bournazos S, Klein F, Pietzsch J, Seaman MS, Nussenzweig MC, and Ravetch JV– 2014. Broadly neutralizing anti-HIV-1 antibodies require Fc effector functions for in vivo activity. Cell 158: 1243–1253. [PubMed: 25215485]
49. Lu CL, Murakowski DK, Bournazos S, Schoofs T, Sarkar D, Halper-Stromberg A, Horwitz JA, Nogueira L, Golijanin J, Gazumyan A, Ravetch JV, Caskey M, Chakraborty AK, and Nussenzweig MC– 2016. Enhanced clearance of HIV-1-infected cells by broadly neutralizing antibodies against HIV-1 in vivo. Science 352: 1001–1004. [PubMed: 27199430]
50. Brunner KT, Hurez D, McCluskey RT, and Benacerraf B– 1960. Blood Clearance of P32-Labeled Vesicular Stomatitis and Newcastle Disease Viruses by the Reticuloendothelial System in Mice. The Journal of Immunology 85: 99–105. [PubMed: 13805345]
51. Wei BL, Denton PW, O'Neill E, Luo T, Foster JL, and Garcia JV– 2005. Inhibition of lysosome and proteasome function enhances human immunodeficiency virus type 1 infection. J. Virol 79: 5705–5712. [PubMed: 15827185]
52. Fredericksen BL, Wei BL, Yao J, Luo T, and Garcia JV– 2002. Inhibition of endosomal/lysosomal degradation increases the infectivity of human immunodeficiency virus. J. Virol 76: 11440–11446. [PubMed: 12388705]
53. Miettinen HM, Rose JK, and Mellman I– 1989. Fc receptor isoforms exhibit distinct abilities for coated pit localization as a result of cytoplasmic domain heterogeneity. Cell 58: 317–327. [PubMed: 2568890]
54. Miettinen HM, Matter K, Hunziker W, Rose JK, and Mellman I– 1992. Fc receptor endocytosis is controlled by a cytoplasmic domain determinant that actively prevents coated pit localization. J. Cell. Biol 116: 875–888. [PubMed: 1734021]

55. Van Den Herik-Oudijk IE, Westerdaal NAC, Henriquez NV, Capel PJA, and van de Winkel JGJ– 1994. Functional analysis of human Fcγ RII (CD32) isoforms expressed in B lymphocytes. J. Immunol 152: 574–584. [PubMed: 8283039]
56. Ahmed SS, Muro H, Nishimura M, Kosugi I, Tsutsui Y, and Shirasawa H– 1995. Fc receptors in liver sinusoidal endothelial cells in NZB/W F1 lupus mice: A histological analysis using soluble immunoglobulin G-immune complexes and a monoclonal antibody (2.4G2). Hepatology 22: 316–324. [PubMed: 7541388]
57. Dekkers G, Bentlage AEH, Stegmann TC, Howie HL, Lissenberg-Thunnissen S, Zimring J, Rispens T, and Vidarsson G– 2017. Affinity of human IgG subclasses to mouse Fc gamma receptors. MAbs 9: 767–773. [PubMed: 28463043]
58. Bruhns P 2012. Properties of mouse and human IgG receptors and their contribution to disease models. Blood 119: 5640–5649. [PubMed: 22535666]
59. Leslie RGQ 1980. Macrophage handling of soluble immune complexes. Use of specific inhibitors to study the biochemical events involved in complex catabolism. Eur. J. Immunol 10: 799–802. [PubMed: 7428807]
60. Knutson DW, Kijlstra A, and Van Es LA– 1977. Association and dissociation of aggregated IgG from rat peritoneal macrophages. J. Exp. Med 145: 1368–1381. [PubMed: 859000]
61. Knutson DW, Kijlstra A, and Van Es LA– 1979. The kinetics for binding and catabolism of aggregated IgG by rat peritoneal macrophages. J. Immunol 123: 2040–2048. [PubMed: 489969]
62. Sips M, Krykbaeva M, Diefenbach TJ, Ghebremichael M, Bowman BA, Dugast AS, Boesch AW, Streeck H, Kwon DS, Ackerman ME, Suscovich TJ, Brouckaert P, Schacker TW, and Alter G– 2016. Fc receptor-mediated phagocytosis in tissues as a potent mechanism for preventive and therapeutic HIV vaccine strategies. Mucosal. Immunol 9: 1584–1595. [PubMed: 26883728]
63. Chung AW, Ghebremichael M, Robinson H, Brown E, Choi I, Lane S, Dugast AS, Schoen MK, Rolland M, Suscovich TJ, Mahan AE, Liao L, Streeck H, Andrews C, Rerks-Ngarm S, Nitayaphan S, de Souza MS, Kaewkungwal J, Pitisuttithum P, Francis D, Michael NL, Kim JH, Bailey-Kellogg C, Ackerman ME, and Alter G– 2014. Polyfunctional Fc-effector profiles mediated by IgG subclass selection distinguish RV144 and VAX003 vaccines. Sci. Transl. Med 6: 228ra238.
64. Chu SY, Vostiar I, Karki S, Moore GL, Lazar GA, Pong E, Joyce PF, Szymkowski DE, and Desjarlais JR– 2008. Inhibition of B cell receptor-mediated activation of primary human B cells by coengagement of CD19 and FcgammaRIIb with Fc-engineered antibodies. Mol. Immunol 45: 3926–3933. [PubMed: 18691763]
65. Horton HM, Chu SY, Ortiz EC, Pong E, Cemerski S, Leung IW, Jacob N, Zalevsky J, Desjarlais JR, Stohl W, and Szymkowski DE– 2011. Antibody-mediated coengagement of FcgammaRIIb and B cell receptor complex suppresses humoral immunity in systemic lupus erythematosus. J. Immunol 186: 4223–4233. [PubMed: 21357255]
66. Margolis DM, Garcia JV, Hazuda DJ, and Haynes BF– 2016. Latency reversal and viral clearance to cure HIV-1. Science 353: aaf6517. [PubMed: 27463679]

Key points:

1. Neutralizing Ab opsonized HIV were cleared faster from blood circulation than HIV
2. FcγRIIb, the lone FcγR expressed in human LSEC clear Ab-HIV via endocytosis
3. Endocytosed Ab-HIV localize to lysosomes of LSEC

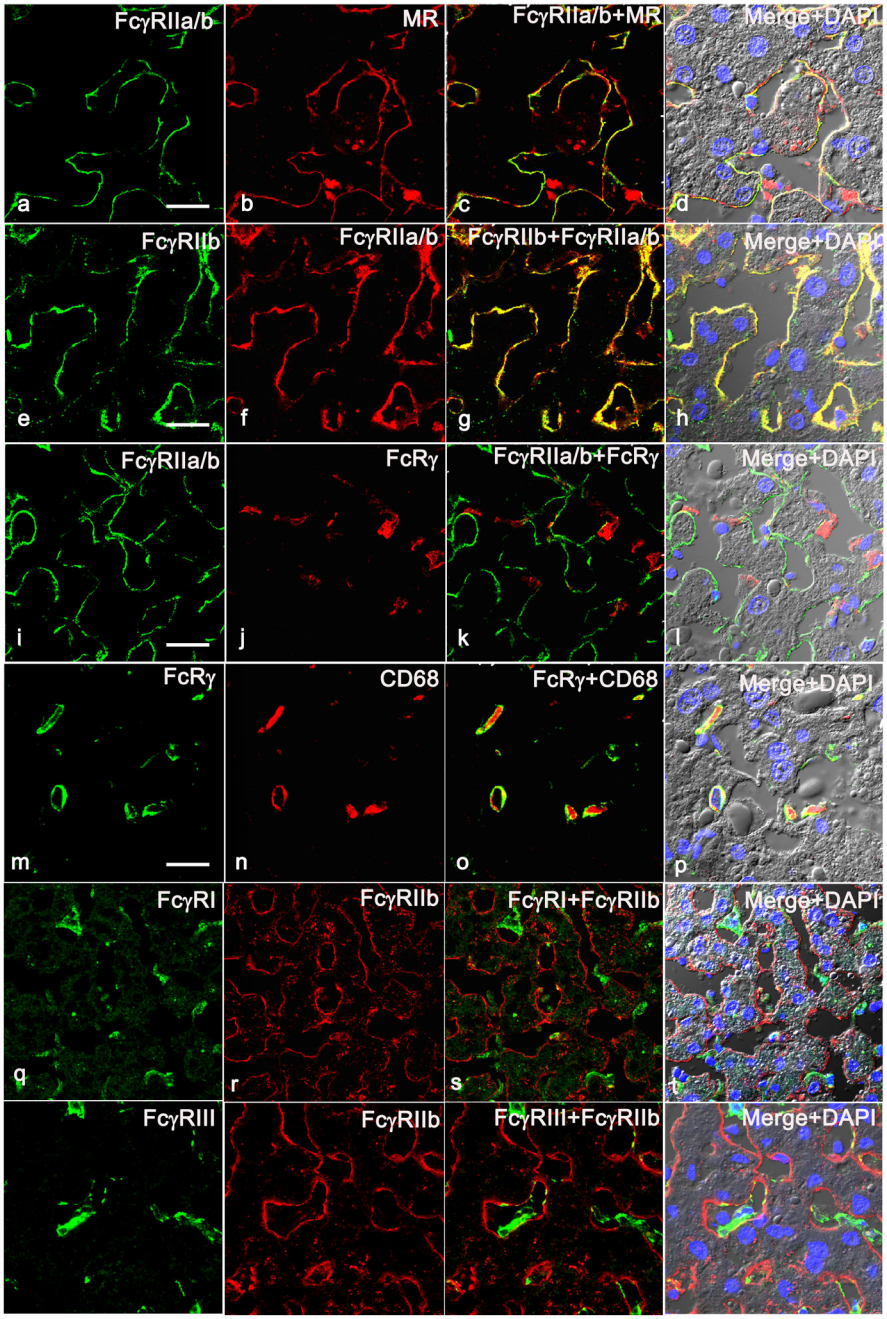

Figure 1. Human LSEC express only FcγRIIb.

Representative three-color immunofluorescence image from three biologically independent human liver samples. The 4 panel top row portrays the expression pattern of FcγRIIa/b in human liver using pan FcγRII mAb KB61 (green) along with LSEC marker anti-mannose receptor (MR) (red). The 2nd row shows the expression of FcγRIIb using pAb 163.96 (green) that colocalizes with mAb KB61 (red). The 3rd row shows the expression of FcγRIIa/b using mAb KB61 (green) along with anti- FcRγ (red). The 4th row illustrates the expression of FcRγ (green) along with KC marker CD68 (red). The 5th row illustrates the expression of FcγRI (green) along with FcγRIIb using pAb 163.96 (red). The 6th row

demonstrates the expression of FcγRIII (green) along with FcγRIIb using pAb 163.96 (red). The column 3 shows the merged image of first two columns. Column 4 shows the merged images of the first two columns along with DIC and DAPI staining of nuclei (blue). The scale bar in 1st column indicates 20μm.

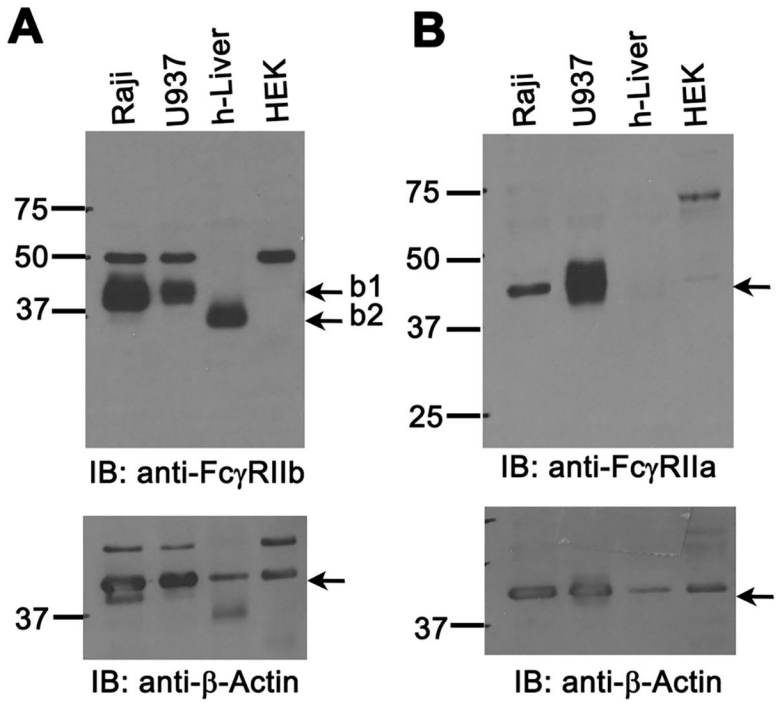

Figure 2. Human liver express more of FcγRIIb than FcγRIIa.

A. An ECL-developed Immunoblot (IB) using rabbit pAb showing FcγRIIb expression in human liver lysates and cell line lysates prepared as described in M&M. Numbers are MW markers in kDa. The IB are representative of data from 3 different human liver samples/ biological replicates. **B**. An ECL-developed IB using rabbit pAb 260 showing FcγRIIa expression in human liver lysates and cell line lysates prepared as described in M&M. Numbers are MW markers in kDa. Numbers are molecular mass markers in kDa. The lower panels of A and B show loading control anti-β-actin. Arrows in top panels point the bands for FcγRIIb isoforms b1 and b2 (Panel A) and FcγRIIa (Panel B).

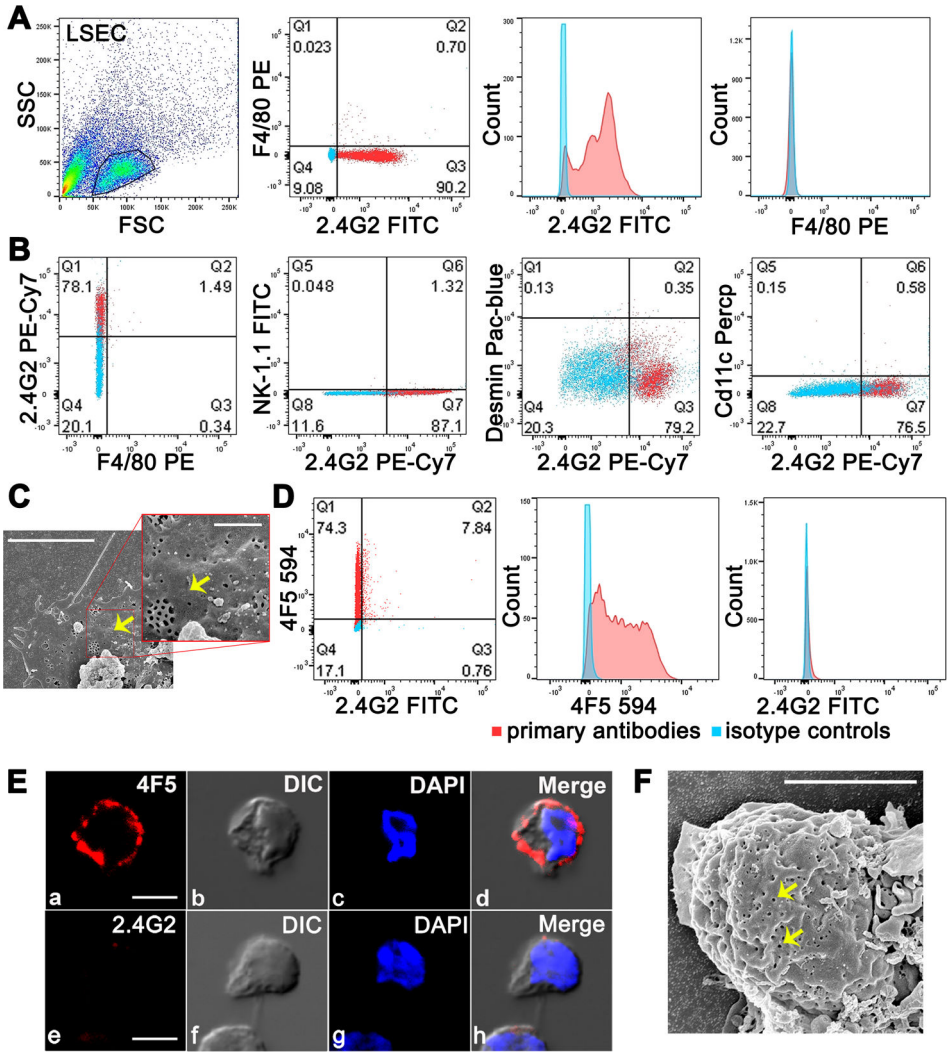

Figure 3. A-C: Flow cytometry analysis confirms purity of isolated mouse LSEC. D-F: LSEC from 2B-KIX mice express human FcγRIIb and not murine FcγRIIb.

A. Representative flow cytometric acquisition plot showing gated LSEC preparation from BALB/c mouse showing two color flow cytometric analysis of 2.4G2 FITC plus F4/80 PE, and histogram representation of single Fluor expression. The results are representative of 4 different experiments and mice/biological replicates. **B.** Five color flow cytometric analysis of gated LSEC from BALB/c mouse for 2.4G2 PE-Cy7, F4/80 PE, NK-1.1 FITC, Desmin Pac-blue, and Cd11c Percp. Two colors analyzed at one given time are shown in one Figure. **C.** The picture shows the SEM image of LSEC from a BALB/c mouse. Arrows point fenestrae. The insert projected represents zoomed view. **D.** Representative two color flow cytometric analysis of gated LSEC from 2B-KIX mouse for 2.4G2 FITC plus 4F5 594 along with histograms showing single colors from 3 different experiments and mice. In A-D, events from isotype controls are represented as blue dots/blue peaks and from primary antibodies as red dots/red peaks. The average percentage of events showing single or double positive expression from three different LSEC preparations is indicated in respective quadrants. **E.** Confocal microscopic image of LSEC from 2BKIX showing labeling of 4F5

(top row) and 2.4G2 (bottom row) along with DIC and DAPI (nucleus). **F.** The picture shows the SEM image of LSEC from a 2B-KIX mouse. Arrows point fenestrae. Note folded and layered cell membranes of LSEC. The scale bar in C, E and F indicates 5μm.

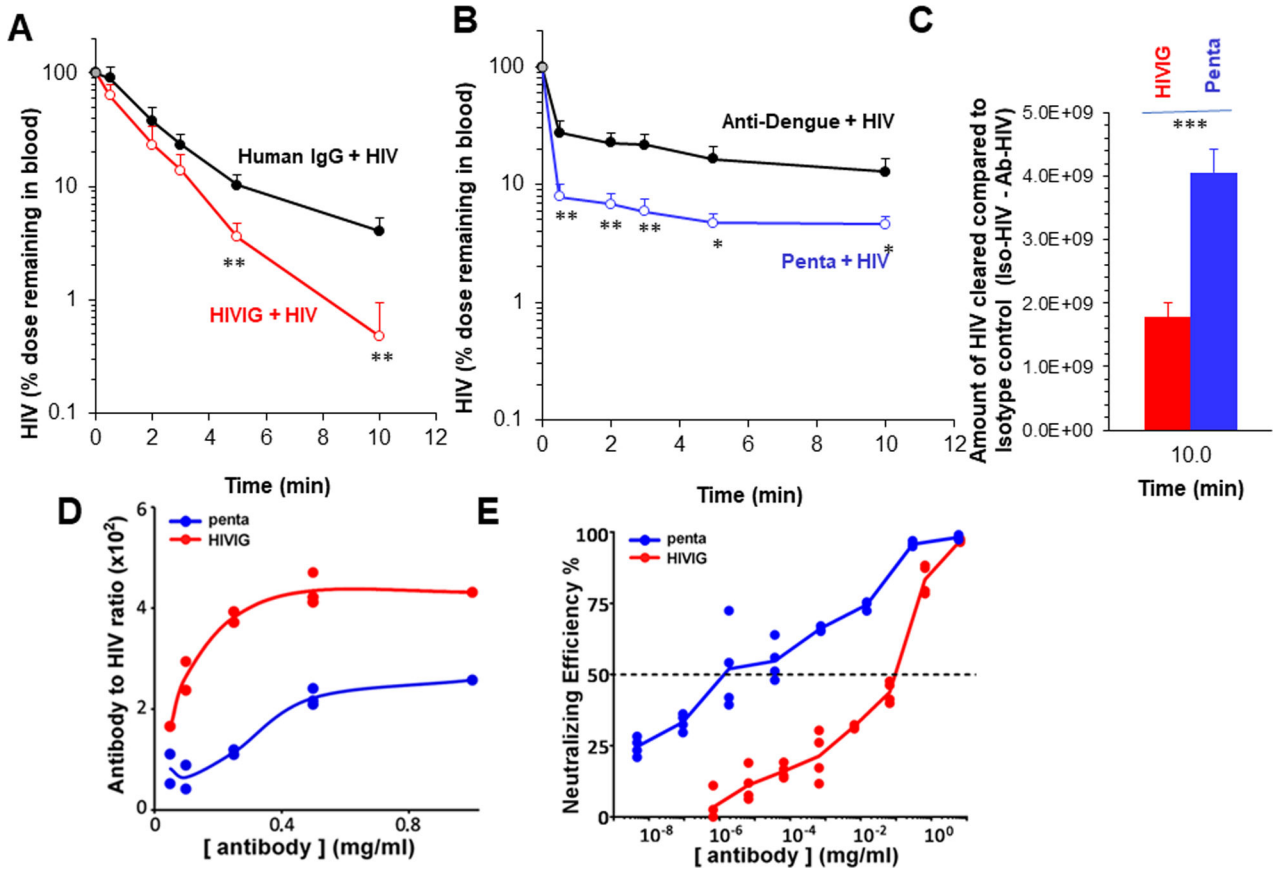

Figure 4. NAbs enhance clearance of HIV from circulation better than HIVIG and Antibody-to-HIV ratio in the immune complexes does not correlate positively with clearance efficiency.

The clearance kinetic curve shows disappearance of Ab-HIV from blood circulation of 2B-KIX mice. Mice were infused by retro-orbital plexus of Ab-HIV prepared using 5×10^{10} HIV and 25mg/kg of either HIVIG or pentamix of Nbs along with their isotype controls namely human IgG or Anti-Dengue IgG, respectively as described in M&M. The clearance curve data are representative of two different experiments with each 4 mice per group/biological replicates. Panel **A** shows clearance of HIVIG-HIV (red open circles) and control human IgG (black closed circles). Panel **B** shows the clearance of pentamix-HIV (blue open circles) and irrelevant isotype control anti-dengue IgG opsonized HIV (black closed circles). The curve describes the HIV particle numbers in blood per mouse cleared over ten min time ± SD using data averaged from 4 different mice. The data in percentage with assumed blood concentration at time zero as 100%. This was based on the injected dose divided by blood volume of a mouse. **C.** Plotted curves describe the difference of HIV blood concentrations ± SD between Ab-HIV and the respective control group at 10 min using data averaged from 4 different mice. **D.** Dose-dependent Ab-HIV binding curves expressing the antibody to HIV ratio for HIVIG (red line) and pentamix (blue line). Representative curves from two different expts (n=2) showing the binding of various concentrations of Alexa-594 labelled Ab to GFP-expressing HIV, which was immobilized on GNA coated plates. The binding ratios were measured and calculated based on the fluorescence units obtained from fluorimeter.

E. Dose-dependent neutralization curves expressing the neutralizing efficiency to HIV for HIVIG (red line) and pentamix of MAbs (blue line). Representative curves from 3 different experiments showing the neutralizing efficiency of various concentrations of antibodies plus 10^8 infectious HIV particles to the TZM-bl cells. The neutralizing efficiency was measured and calculated based on the luminescence units generated by luciferase reaction from infected cells.

Values of all significant correlations ($p<0.05$) are given with degree of significance indicated (* $p<0.05$, ** $p<0.01$, *** $p<0.001$) by students t-test.

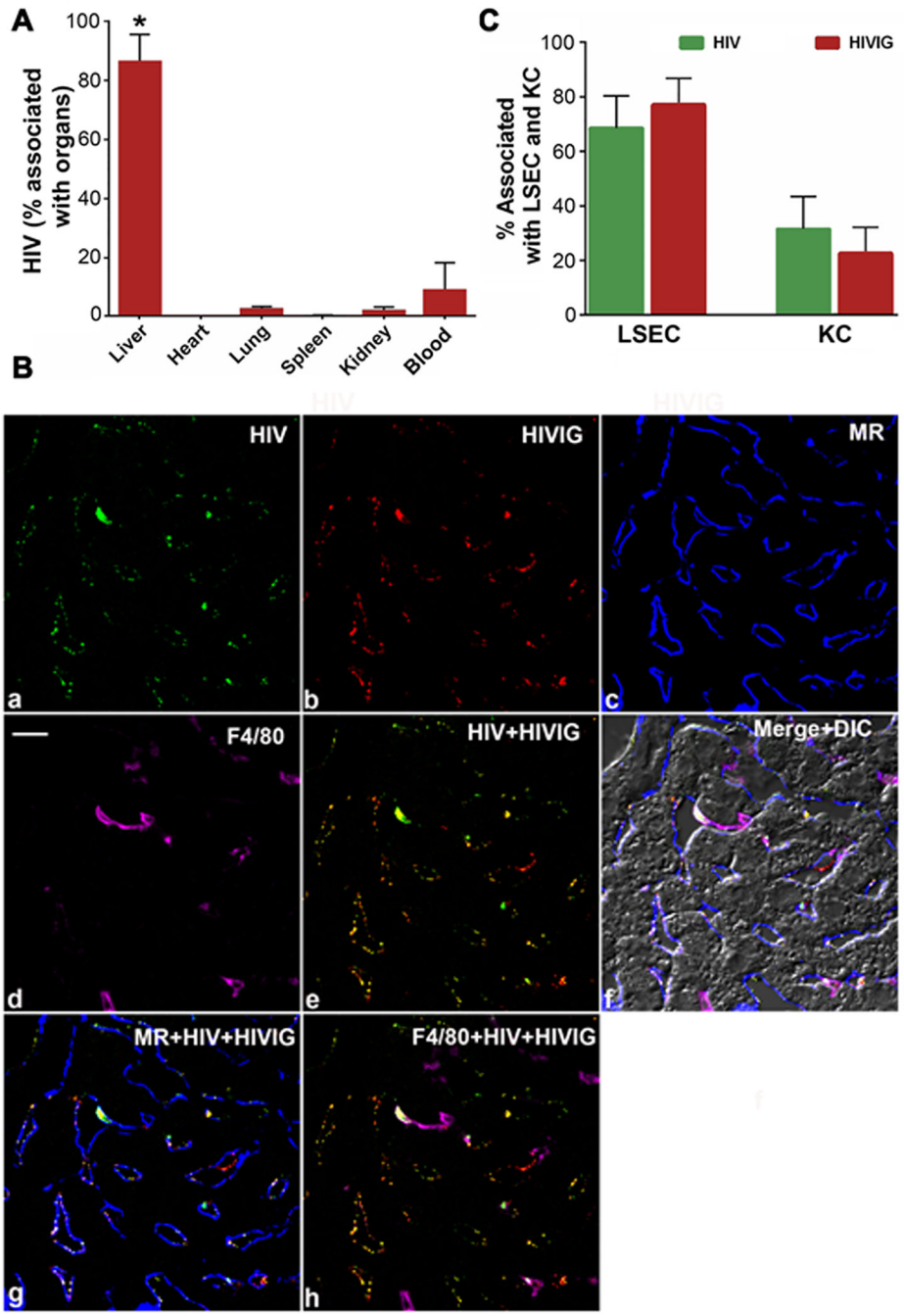

Figure 5. A. Liver is the major organ that clears antibody opsonized HIV. B-C. In liver, HIVIG-HIV immune complex is distributed primarily to LSEC.

A. The bar graph shows the distribution percentage of HIVIG-HIV to various organs including blood after factoring total organ weight ± SD from 3 different mice. The * represents a p value of 0.05 by students t-test. **B.** Four-color confocal fluorescence microscopic image of 5μm liver section from 2B-KIX mice after 3 min infusion of immune complex made of HIV-488 and HIVIG-594. a. Green puncta identify HIV particles. b. Red puncta identifies HIVIG. c. Mannose receptor (MR) labelled in blue color outlines LSEC. d.

F4/80 in magenta color delineates KC. e. Merged a and b. f. Merged a-d plus DIC. Scale bar in a panel indicates 10μm. **C**. Bar graph showing quantitative colocalization analysis of 30 images from 3 mice/biological replicates similar to the image represented in A. The graph shows the percentage of HIV (green puncta) and HIVIG (red puncta) colocalizing with signal from LSEC marker MR (blue) and KC marker (magenta).

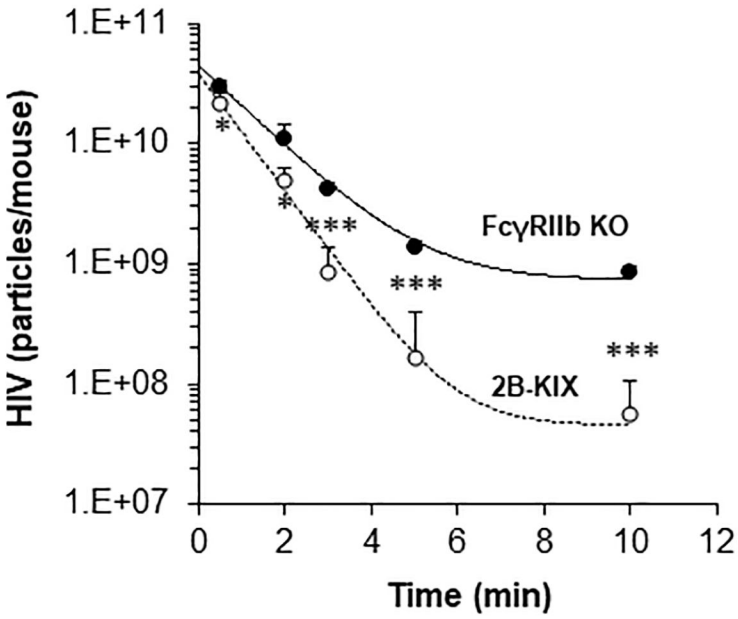

Figure 6: Human FcγRIIb mediates clearance of HIVIG-opsonized HIV.

Clearance kinetics showing disappearance of HIVIG-HIV from blood circulation of 2B-KIX mouse (red open circle) and FcγRIIb KO (black closed circle). Mice were infused by retro-orbital plexus of HIVIG-HIV prepared using 5×10^{10} HIV and 50mg/kg of HIVIG. The curve describes the HIV particle numbers in blood per mouse cleared over ten min time ± SD using data averaged from 4 different mice/biological replicates. The data was drawn using a 1/Y prediction weighting decay model to smooth the connection of data points. Values of all significant correlations ($p<0.05$) are given with degree of significance indicated (* $p<0.05$, ** $p<0.01$, *** $p<0.001$) by students t-test.

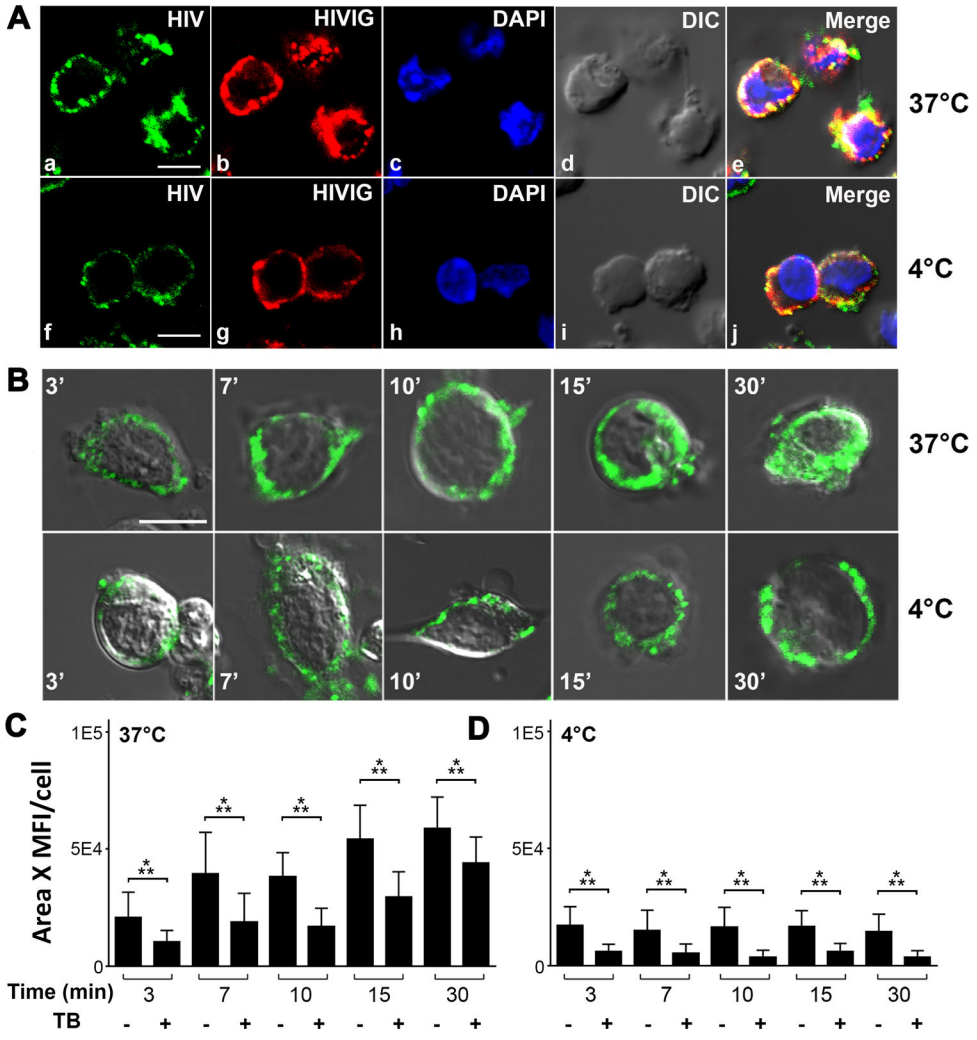

Figure 7. LSEC bind and endocytose HIVIG-HIV Immune complex.

A. Three-color fluorescence microscopic image of PFA fixed LSEC from 2BKIX mice, which where incubated with HIV-488 plus HIVIG-594 immune complex (IC) at 37°C/4°C for 30 min. (a, f) Green puncta identify HIV particles. (b, g) Red puncta identifies HIVIG. (c, h) DAPI (blue) identifies nucleus. (d, i) DIC (e, j) Merged (a)–(d)/(f)–(i). (a-e) Confocal microscopy images showing endocytosis of LSEC at 37°C, (f-j) confocal microscope images showing binding of HIV-488 plus HIVIG-594 IC by LSEC at 4°C. Scale bar indicates 5μm. **B.** Live cell confocal microscopic image of LSEC from 2B-KIX mice incubated with HIV plus HIVIG-FITC IC for various time points from 3 to 30 min at 37°C (top panel) and 4°C (bottom panel). Green puncta identify HIVIG FITC. **C.** Bar graph showing quantification of green puncta of HIV plus HIVIG-FITC IC from 25 live cell confocal microscopic images with and without trypan blue is shown here. The mean fluorescence intensity and the total pixel area of green puncta were measured and plotted. A total of 400 LSEC from three different mice/biological replicate were analyzed. Bar graphs show average fluorescence intensity and mean± SD per cell. Values of all significant correlations ($p<0.05$) are given with degree of significance indicated (* $p<0.05$, ** $p<0.01$, *** $p<0.001$) by students t-test.

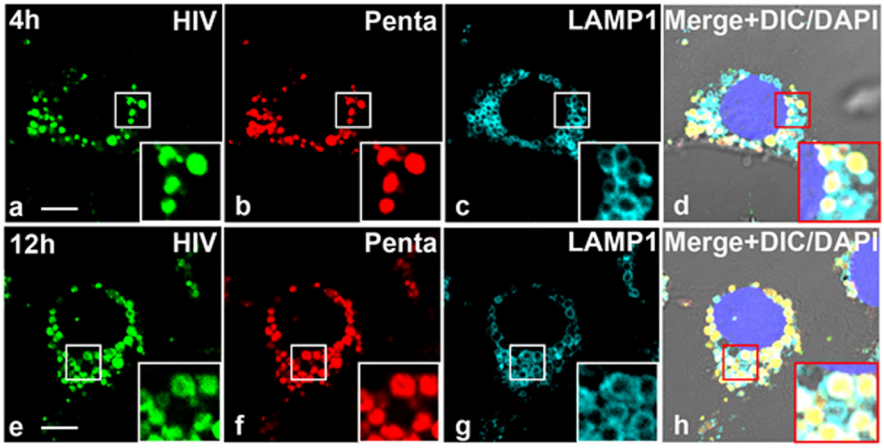

Figure 8. HIV-Pentamix immune complex localizes within lysosomes of LSEC.

A. Four-color fluorescence microscopic image of LSEC from 2B-KIX mice incubated with 488-HIV–647-Penta complex at 37°C and immunolabelled with anti-LAMP-1 antibody at 4hrs (Top Panel) and 12h (bottom panel). The data are representative of 15 images from two different mice/biological replicates. (a,e) Green puncta identify 488-HIV particles. (b,f) Pseudo colored Red puncta identifies 647-Penta mix. (c,g) Pseudo colored cyan identifies lysosome membrane structure marked by anti-LAMP-1 Ab. (d) Merged (a)–(c) plus DAPI stained nuclei and DIC. The scale bar represents 5 μm.